CELLULAR NEUROSCIENCE

Regulation of membrane homeostasis by TMC1 mechanoelectrical transduction channels is essential for hearing

Angela Ballesteros* and Kenton J. Swartz*

The mechanoelectrical transduction (MET) channel in auditory hair cells converts sound into electrical signals, enabling hearing. Transmembrane-like channel 1 and 2 (TMC1 and TMC2) are implicated in forming the pore of the MET channel. Here, we demonstrate that inhibition of MET channels, breakage of the tip links required for MET, or buffering of intracellular Ca^{2+} induces pronounced phosphatidylserine externalization, membrane blebbing, and ectosome release at the hair cell sensory organelle, culminating in the loss of TMC1. Membrane homeostasis triggered by MET channel inhibition requires *Tmc1* but not *Tmc2*, and three deafness-causing mutations in *Tmc1* cause constitutive phosphatidylserine externalization that correlates with deafness phenotype. Our results suggest that, in addition to forming the pore of the MET channel, TMC1 is a critical regulator of membrane homeostasis in hair cells, and that *Tmc1*-related hearing loss may involve alterations in membrane homeostasis.

INTRODUCTION

Auditory and vestibular hair cells of the inner ear are the sensory cells responsible for perceiving sound and head movements, respectively. The mechanosensory apparatus consists of a bundle of 50 to 100 specialized actin-based microvilli, termed stereocilia, at the apical region of hair cells (*1*). In mammals, stereocilia are arranged in three rows of increasing height interconnected by several protein filaments, including the tip link that transfers mechanical stimuli to the mechanoelectrical transduction (MET) channels (*2*). After sound stimulation, the stereocilia are deflected toward the tallest stereocilia row, opening the MET channel and leading to depolarization of the hair cell and conversion of the mechanical stimulus into an electrical response (*3*).

Five integral membrane proteins have been proposed to be components of the hair cell MET channel complex: the transmembrane-like channel 1 and 2 proteins (TMC1 and TMC2), LHFPL5, protocadherin-15, and TMIE (*4*–*8*). Of those, TMC1 and TMC2 have been recently identified as pore-forming subunits of the MET channel (*4*, *9*) and reported to exhibit channel activity when reconstituted in liposomes (*10*). Mammalian auditory hair cells express both *Tmc1* and *Tmc2*, but their expression patterns vary during development, and they confer different properties to the MET channel (*5*, *11*, *12*). Expression of *Tmc2* is insufficient for maintaining normal hearing in mice lacking *Tmc1* (*13*, *14*), suggesting that TMC1 must have additional functions required for hearing. More than 30 autosomal dominant (DFNA36) and recessive (DFNB7/11) mutations in the *Tmc1* gene cause deafness in humans, highlighting the importance of TMC1 in sound transduction (*15*, *16*). In contrast, no deafness-causing mutations have been identified in *Tmc2*. The dominant M412K and D569N and the recessive D528N *Tmc1* mutations have been extensively characterized in mice (*5*, *17*–*22*). When comparing heterozygous mice for these three *Tmc1* mutations, $Tmc1^{D528N/+}$ mice have normal hearing, whereas $Tmc1^{D569N/+}$ and $Tmc1^{M412K/+}$ mice present hearing loss, consistent with the recessive and dominant nature of these mutations (*18*–*20*). However, the MET channel properties of recessive $Tmc1^{D528N/+}$ hair cells are altered to a similar extent compared to those carrying one copy of the dominant mutations (*17*, *19*, *20*), suggesting that alterations in the functional properties of the MET channel are not sufficient to explain the deafness phenotype of $Tmc1^{D569N/+}$ and $Tmc1^{M412K/+}$ mice. Thus, the molecular mechanisms of *Tmc1*-related deafness remain enigmatic.

We and others have previously reported that TMC proteins are evolutionarily and structurally related to TMEM16, a family of Ca^{2+}-activated lipid scramblases and channels (*4*, *23*–*26*), some of which function as Ca^{2+}-activated chloride channels (*27*). Lipid scramblases provide a permeation pathway for the diffusion of phospholipids between the plasma membrane leaflets following their concentration gradient. Therefore, activation of a lipid scramblase results in the externalization of phosphatidylserine (PS), which is usually restricted to the inner leaflet, and loss of the phospholipid asymmetry at the plasma membrane, a hallmark of many relevant biological processes such as apoptosis, blood coagulation, myoblast fusion, fertilization, synapse pruning, or photoreceptor disc shedding (*28*). A structural model of TMC1 based on *Nectria haematococca* TMEM16, which functions as lipid scramblase and ionic channel (*29*), suggested that TMC1 has a cavity located at the protein-membrane interface that could function as the permeation pathway of the inner ear hair cell MET channel (*4*, *23*). An equivalent cavity in TMEM16s is implicated in the transport of ions and lipids, which are thought to occur through a similar, but not identical, pathway (*30*, *31*).

Inspired by this TMC-TMEM16 relation and by previous work on the ability of aminoglycoside inhibitors of the MET channel to trigger PS externalization and membrane blebbing in hair cells (*32*–*35*), here, we investigated the potential role of TMC proteins in lipid scrambling and regulation of hair cell membrane homeostasis using Airyscan super-resolution confocal microscopy and 13 different transgenic mouse lines. We found that pharmacological inhibition of the MET channel, breakage of the tip links, or buffering of

Molecular Physiology and Biophysics Section, Porter Neuroscience Research Center, National Institute of Neurological Disorders and Stroke, National Institutes of Health, Bethesda, MD 20892, USA.
*Corresponding author. Email: angela.ballesteros@nih.gov (A.B.); swartzk@ninds.nih.gov (K.J.S.)

intracellular Ca^{2+} triggers PS externalization and the formation of PS-positive membrane blebs at the stereocilia and apical hair cell region in a *Tmc1*-dependent and *Tmc2*-independent manner. Furthermore, we report that hair cells impaired by *Tmc1* deafness–causing mutations display constitutive PS externalization, emphasizing the importance of membrane homeostasis for hearing. Our findings show that constitutive PS externalization in *Tmc1* dominant and recessive mutations correlates with the deafness phenotype of these mice, revealing a previously unidentified role for *Tmc1* in the regulation of hair cell membrane homeostasis that is essential for hearing.

RESULTS

Blockage of MET channels triggers PS externalization and membrane blebbing

Rapid PS externalization and membrane blebs have been previously observed at the apical region of hair cells treated with ototoxic aminoglycoside antibiotics, which are well-known inhibitors of the MET channel (*32*, *33*). To examine whether this dysregulation of membrane homeostasis is caused by the blockage of the MET current at rest (*36*), we examined the induction of PS externalization and membrane blebbing in hair cells treated with the aminoglycoside neomycin and with two other non-ototoxic and well-established MET channel blockers, benzamil and curare (*37*–*39*). For this purpose, externalized PS at the cell membrane was detected using the PS-specific binding protein annexin V (AnV) and the overall hair cell surface was visualized by staining with fluorescently labeled wheat germ agglutinin (WGA), which does not affect MET currents (*40*, *41*). To visualize the membrane, we systematically performed parallel experiments in $mT/mG^{Tg/+}$ mice expressing one copy of the membrane-targeted tandem dimer tomato (mtdTomato) fluorescent reporter, which retains functional MET (*42*).

Untreated cochlear hair cells from 6-day-old (P6) mice show no specific labeling of AnV (Fig. 1, A to D), indicating that PS is not exposed on these cells. However, 25-min incubation with 100 μM neomycin, benzamil, or the less permeable antagonist curare (*37*, *38*, *43*) triggered robust PS externalization at the apical hair cell region in wild-type (Fig. 1, A and B) and $mT/mG^{Tg/+}$ mice (Fig. 1, C and D). Neomycin and benzamil induced PS externalization in both outer (OHCs) and inner hair cells (IHCs), whereas curare-induced PS externalization was mainly restricted to OHCs. Because the IC_{50} (median inhibitory concentration) of curare for inhibiting MET was estimated in murine OHCs (*37*) and higher curare concentration may be needed to fully block the MET channels in IHCs, we performed experiments with 1 mM curare. Higher curare concentration induced robust PS externalization in both OHCs and IHCs (fig. S3) like that observed with the other two well-established MET channel blockers. These data demonstrate that three chemically distinct MET inhibitors trigger PS externalization.

In addition to PS externalization, neomycin is known to induce membrane blebbing and increase hair cell capacitance, indicating that PS externalization is accompanied by membrane addition to the hair cell surface (*32*, *44*) and agreeing with previous work on other cell types describing a relationship between PS externalization and membrane blebbing (*45*–*47*). Consistent with this precedence, we found that while the mtdTomato reporter labeled the membrane homogeneously in untreated hair cells isolated from $mT/mG^{Tg/+}$ mice, it was enriched in vesicle-like structures and membrane blebs in hair cells treated with neomycin, benzamil, or curare (Fig. 1C and fig. S1). In addition, we observed an increase in the mtdTomato fluorescence intensity in OHCs and IHCs treated with neomycin, benzamil, or curare (Fig. 1E and fig. S3), which parallels the changes in AnV signal (Fig. 1D). These data indicate that inhibition of the MET channel leads to membrane addition and blebbing at the apical region of hair cells.

The WGA labeling and the resolution provided by the Airyscan LSM 880 confocal microscope allowed us to pinpoint the externalized PS. Neomycin is known to induce PS externalization at the stereocilia, around the apical surface of the hair cell, and at the kinocilial area (*32*). Accordingly, we observed that treatment with benzamil, neomycin, or curare led to PS externalization at these same regions. Hair cells treated with neomycin presented larger AnV-positive patches around the hair cells and at the kinocilial area than the other treatments (figs. S1 and S2, blue arrows). These AnV-positive patches or vesicles were also enriched with mtdTomato, suggesting that PS externalization and membrane blebbing are related as previously reported (*45*–*47*). We observed that externalized PS and mtdTomato accumulate at the tips of the shorter stereocilia rows (fig. S2, green arrows), where TMC1, TMC2, and the MET channel are located (*48*, *49*). Vesicle-like particles labeled with WGA, AnV, and mtdTomato were observed bulging at the tips of the stereocilia and around the hair cell surface (figs. S1 and S2, yellow arrows), indicating outward budding and vesiculation of the membrane.

We also attempted to see evidence of the formation of AnV-positive patches, blebs, and vesicles upon blockage of the MET in live-cultured wild-type hair cells labeled with the membrane marker CellMask. AnV specifically detected externalized PS at the hair cell bundle of curare-treated cells but not in the untreated hair cells (Fig. 1F). AnV and CellMask-positive patches, blebs, and vesicles were observed at the tips of the stereocilia and floating near the stereocilia bundle in treated samples (Fig. 1G). The average diameter of free vesicles (1.05 ± 0.27 μm) was larger than that of stereocilia-attached vesicles (0.55 ± 0.28 μm), which suggests that these vesicles are ectosomes shedding from the stereocilia membrane (*50*). That we observed PS externalization, membrane blebbing, and vesicle release in both fixed and live tissue suggests that these events are unlikely to arise from an experimental artifact related to tissue fixation. We conclude that pharmacological inhibition of the MET channel leads to PS externalization, membrane blebbing, and ectosome release in the apical region of murine auditory hair cells, suggesting that blockage of the MET channel is accompanied by dysregulation of the apical hair cell membrane homeostasis.

Tip link disruption leads to PS externalization and membrane blebbing

We next explored whether manipulations that mechanically disturb the MET channel current would also trigger PS externalization. For this purpose, we analyzed PS externalization and membrane blebbing in hair cells from P6 $mT/mG^{Tg/+}$ mice treated with Hanks' balanced salt solution (HBSS; control) or 5 mM BAPTA [1,2-bis(2-aminophenoxy) ethane-*N*,*N*,*N*′,*N*′-tetraacetic acid] in Ca^{2+}- and Mg^{2+}-free HBSS (HBSS-CFM), a manipulation established to break the tip links that mechanically gate the MET channel (*2*, *51*). We found a robust PS externalization and accumulation of AnV and mtdTomato fluorescence signals at the stereocilia, vestigial kinociliary site, and blebs in BAPTA-treated hair cells but not in the control (Fig. 2A). In addition, AnV and mtdTomato fluorescence intensities were increased in BAPTA-treated hair cells (Fig. 2, B and C). Comparable results were

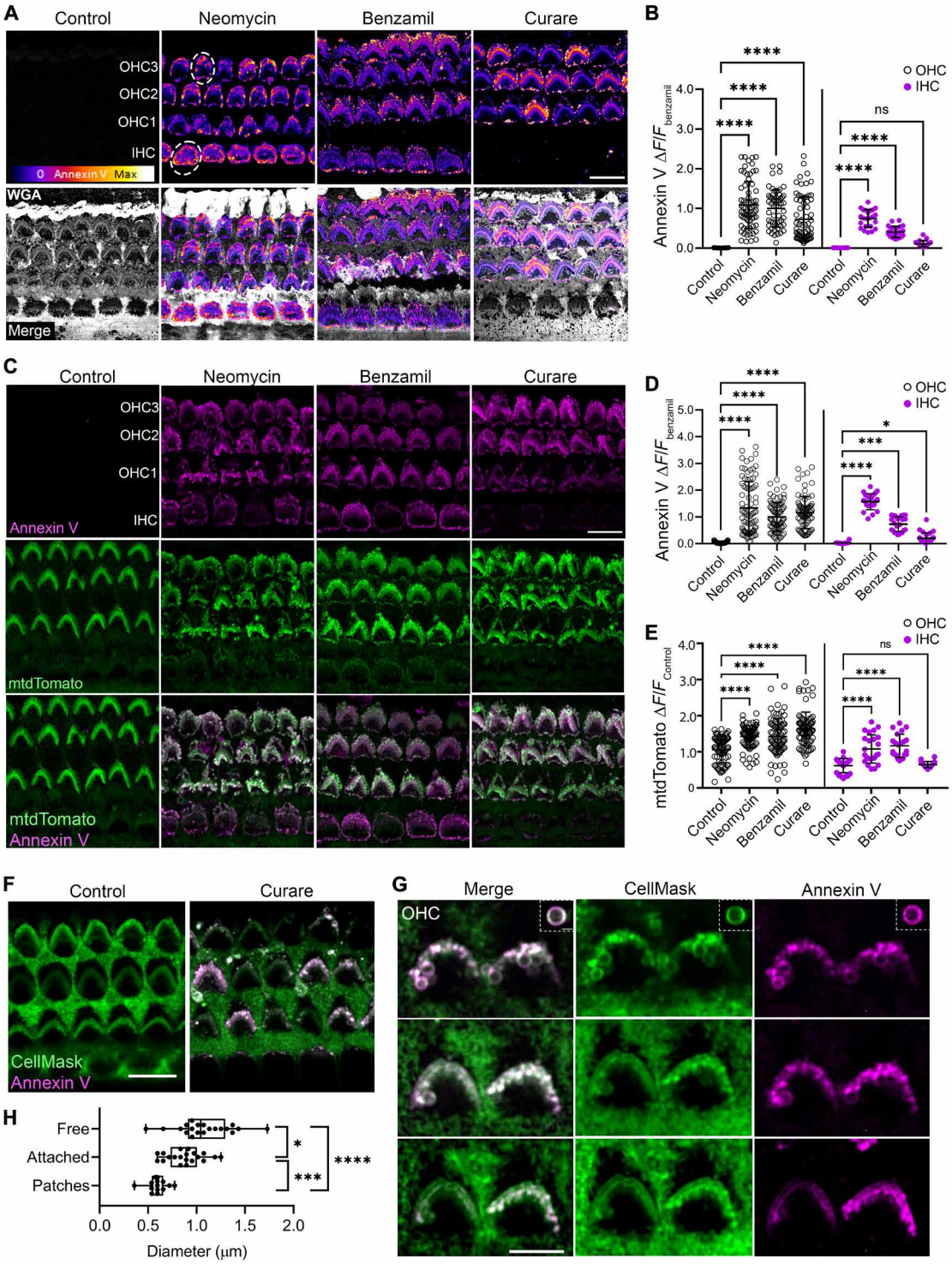

Fig. 1. Blockade of the MET channel triggers PS externalization and membrane blebbing. (**A**) Confocal images of P6 wild-type hair cells incubated with WGA (gray) and AnV in the absence (control) or presence of 100 μM neomycin, benzamil, or curare. (**B**) Quantification of AnV fluorescence intensity in OHCs (○) or IHCs (●) treated as in (A). (**C**) Confocal images of P6 mT/mG$^{Tg/+}$ hair cells expressing the mtdTomato membrane reporter (green) treated as in (A). Quantification of the AnV (**D**) or mtdTomato (**E**) fluorescence intensity in IHCs and OHCs treated as in (C). (**F**) Live imaging of wild-type hair cells labeled with CellMask (green) and AnV (magenta) in the absence (control) or presence of curare. (**G**) Confocal planes of OHCs treated with curare as in (F). (**H**) Diameter of AnV-positive vesicles ($n = 20$). In (B), (D), and (E), mean ± SD is shown for $n = 70$ to 85 OHCs and 22 to 27 IHCs from two cochleae. One-way analysis of variance (ANOVA) analysis was performed (ns $P > 0.05$, *$P < 0.05$, ***$P < 0.001$, and ****$P < 0.0001$). Scale bars, 10 μm in (A), (C), and (F) and 5 μm in (G). See also figs. S1 to S3.

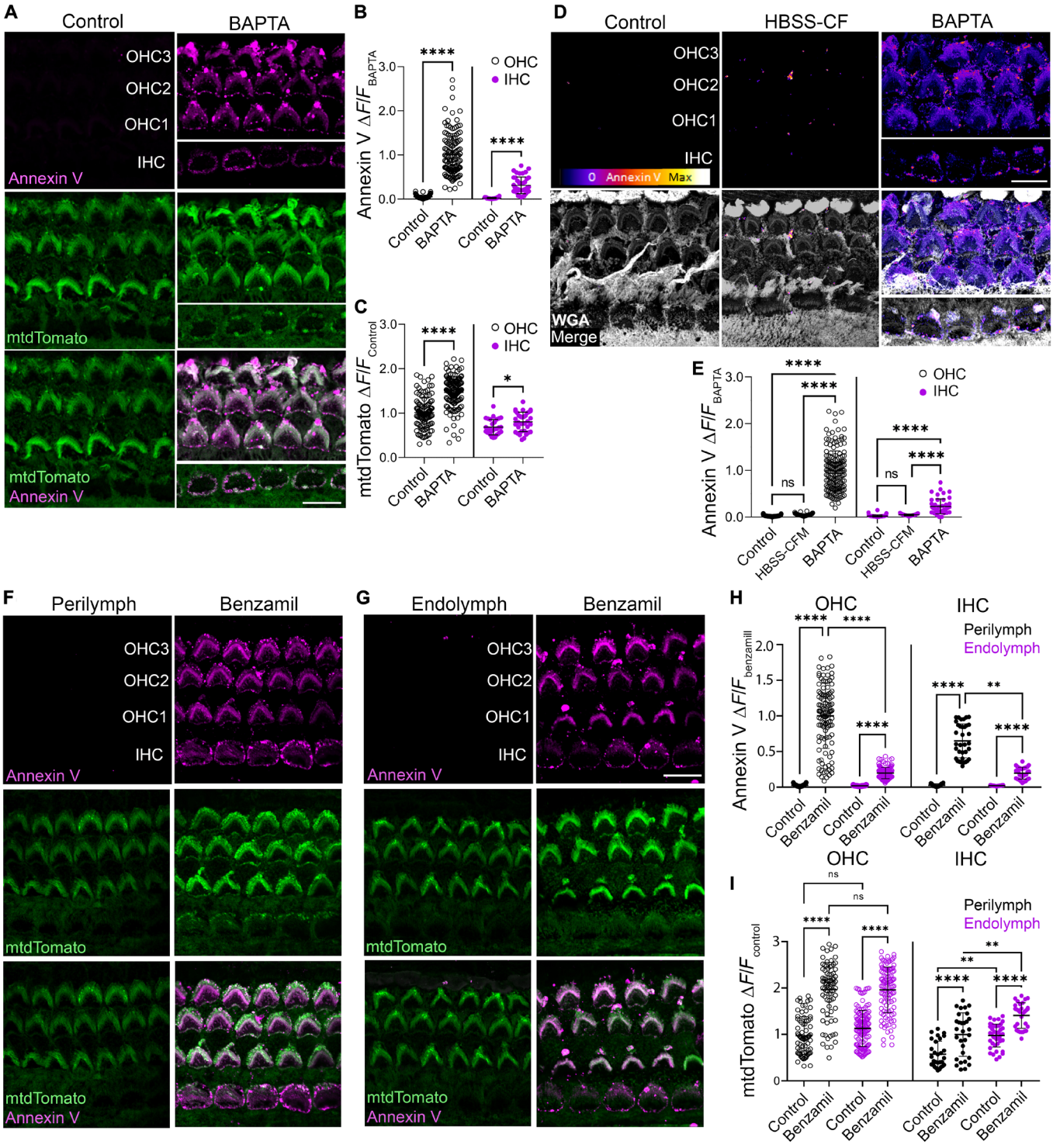

Fig. 2. PS externalization and membrane blebbing after tip link disruption and in biological extracellular solutions. (**A**) Confocal images of P6 mT/mG$^{Tg/+}$ hair cells expressing mtdTomato (green) treated with HBSS (control) or 5 mM BAPTA before the addition of AnV (magenta). Quantification of the AnV (**B**) and mtdTomato (**C**) fluorescence intensity at the apical region of OHCs (○) and IHCs (●) treated as in (A). (**D**) Confocal images of wild-type hair cells treated with HBSS (control), HBSS cation-free medium (HBSS-CFM), or 5 mM BAPTA in HBSS-CFM containing WGA (gray) before the addition of AnV (Fire LUT). (**E**) AnV fluorescence intensity quantification as in (D). (**F**) Confocal images of P6 mT/mG$^{Tg/+}$ mice hair cells untreated or treated with 100 μM benzamil in perilymph-like buffer containing AnV. (**G**) Confocal images of P6 mT/mG$^{Tg/+}$ hair cells untreated or treated with 100 μM benzamil in endolymph-like buffer containing AnV. Quantification of AnV (**H**) and mtdTomato (**I**) fluorescence intensity as in (F) and (G). In (B), (C), (E), (H), and (I), mean fluorescence intensity ± SD is represented for $n = 82$ to 126 OHCs and 19 to 43 IHCs from two cochleae. Unpaired t test (B and C) or one-way ANOVA analysis (E, H, and I) was performed (ns $P > 0.05$, *$P < 0.05$, **$P < 0.01$, and ****$P < 0.0001$). Scale bar, 10 μm. See also fig. S4.

obtained in hair cells from P6 wild-type mice (Fig. 2, D and E). We did not detect AnV labeling in hair cells incubated in HBSS-CFM alone (Fig. 2D), indicating that the PS externalization observed in BAPTA-treated cells was not caused by the low cation concentration of this buffer. Like our observations with the MET blockers, AnV staining was more robust in OHCs than in IHCs (Fig. 2, B and E). It is important to note that due to the Ca^{2+}-dependent PS binding of AnV, cochlear explants were incubated for 5 min in HBSS containing AnV after BAPTA treatment. Although the regeneration of the tip links takes hours (*52*, *53*), we wanted to confirm these results using a recombinant C2 domain of lactadherin/MFG-E8 fused to the fluorescent protein clover (clover- Lact-C2), which binds PS in the absence of Ca^{2+} (*54*). Consistent with the AnV results, clover-Lact-C2 labeling was detected in BAPTA-treated cells but not in the control (fig. S4, A and B), further supporting the specific detection of externalized PS in response to tip link disruption. Last, to test whether our BAPTA treatment might nonspecifically damage hair cells, we performed FM1-43 uptake experiments and observed robust uptake in control hair cells, similar to previous studies (*12*), yet no detectable uptake following BAPTA treatment (fig. S4, D and E), indicating that this manipulation disrupts MET without damaging the hair cell membrane. Together, these data indicate that pharmacological inhibition of the MET channel or manipulations established to break the tip links required for functional MET are both sufficient to trigger PS externalization.

PS externalization and membrane remodeling occur in perilymph-like conditions

Most of our experiments were performed in HBSS containing 1.26 mM Ca^{2+}. However, in the intact cochlea, the apical hair cell region is immersed in an endolymph solution rich in Na^+ and K^+ and low in Ca^{2+}, whereas the basal region is bathed in perilymph with an ion composition similar to HBSS (*55*). Thus, we next tested whether PS externalization occurs in a physiological environment by incubating hair cells from P6 mT/mG$^{Tg/+}$ mice with AnV in perilymph (1.3 mM Ca^{2+}) or endolymph buffer (25 μM Ca^{2+}) in the absence or presence of 100 μM benzamil. In the absence of benzamil, we did not detect externalized PS in explants incubated in either perilymph or endolymph buffer, indicating that reduced extracellular Ca^{2+} concentrations alone do not trigger PS externalization (Fig. 2, F to H), consistent with our data with HBSS-CFM (Fig. 2, D and E). However, MET blockade with benzamil triggered PS externalization in hair cells immersed in either perilymph or endolymph buffer (Fig. 2, F to H). While the increase in mtdTomato fluorescence intensity was similar in benzamil-treated samples, AnV signal in the endolymph buffer was lower than in the perilymph buffer (Fig. 2, H and I). Therefore, although extracellular Ca^{2+} influences the extent of PS externalization, these results indicate that PS externalization and membrane blebbing occur under physiological ionic conditions.

Transgenic mice lacking functional MET channels fail to externalize PS and remodel the membrane

The results thus far demonstrated that physical and pharmacological disruption of MET triggers PS externalization and membrane blebbing, suggesting that functional MET channels are required for maintenance of membrane homeostasis. To test this hypothesis, we examined PS externalization in response to MET channel blockers in hair cells from *Tmc1* and *Tmc2* double knockout mice (*Tmc1*$^{-/-}$;*Tmc2*$^{-/-}$), which lack functional MET channels (*12*). Furthermore, we generated a triple transgenic mT/mG$^{Tg/+}$ *Tmc1*$^{-/-}$;*Tmc2*$^{-/-}$ mouse expressing the mtdTomato reporter to visualize the hair cell membrane. As previously reported (*12*), we found that the morphology of *Tmc1*$^{-/-}$;*Tmc2*$^{-/-}$ hair cell bundles was altered; IHCs presenting additional stereocilia rows and OHCs were arranged in a "U" shape (fig. S5E). Hair cells from mT/mG$^{Tg/+}$;*Tmc1*$^{-/-}$;*Tmc2*$^{-/-}$ (Fig. 3, A and C) or *Tmc1*$^{-/-}$;*Tmc2*$^{-/-}$ mice (fig. S5, A to D) were incubated with different MET blockers, but in contrast to our results with wild-type hair cells, treatment with neomycin, benzamil, or curare failed to trigger PS externalization in hair cells from these two MET-lacking mouse lines (Fig. 3, A to C, and fig. S5, A and D). Furthermore, we did not observe any alteration of the apical hair cell membrane or an increase of the mtdTomato fluorescence intensity upon MET blockage in mT/mG$^{Tg/+}$;*Tmc1*$^{-/-}$;*Tmc2*$^{-/-}$ hair cells (Fig. 3, A to C), suggesting that *Tmc1* and/or *Tmc2* are required for membrane remodeling after MET channel blockade. In addition, we analyzed PS externalization after benzamil treatment in hair cells from P6 homozygous mT/mG mice (mT/mG$^{Tg/Tg}$), which, unlike their heterozygous counterparts, present profound hearing loss and lack functional MET channels as indicated by their absence of distortion product otoacoustic emissions and failure to uptake the MET channel-permeable FM1-43 dye (*42*). As shown in Fig. 3 (D and E), wild-type and mT/mG$^{Tg/+}$ hair cells externalized PS upon benzamil treatment, whereas benzamil-treated hair cells from mT/mG$^{Tg/Tg}$ littermates failed to externalize PS. Furthermore, mtdTomato fluorescence intensity increased after benzamil treatment in mT/mG$^{Tg/+}$ hair cells but not in cells from mT/mG$^{Tg/Tg}$ mice (Fig. 3F). Thus, we conclude that functional MET is required for PS externalization and apical hair cell membrane remodeling after MET inhibition.

Tmc1, but not *Tmc2*, is essential for PS externalization and membrane blebbing

Because both TMC1 and TMC2 form functional MET channels (*5*, *10*, *12*), we next evaluated the individual role of TMC1 and TMC2 in PS externalization and membrane blebbing. For this purpose, we first analyzed PS externalization in hair cells from *Tmc1*$^{-/-}$ or *Tmc2*$^{-/-}$ mice in an mT/mG$^{Tg/+}$ (Fig. 4, A to F) or wild-type (fig. S5, B to D) background at P6, when both TMC1 and TMC2 contribute to functional MET (*12*). In the absence of MET blockers (control), AnV staining was not detected in *Tmc1*$^{-/-}$ or *Tmc2*$^{-/-}$ hair cells (Fig. 4, A, B, D, and E, and fig. S5, B to D), indicating that the absence of TMC1 or TMC2 does not itself trigger PS externalization. However, like in wild-type hair cells, treatment with neomycin, benzamil, and curare induced PS externalization and an increase of the mtdTomato signal in hair cells from *Tmc2*$^{-/-}$ mice (Fig. 4, A to C, and fig. S5, C and D). In contrast, hair cells from *Tmc1*$^{-/-}$ mice failed to externalize PS after MET channel blockade (Fig. 4, D and E, and fig. S5, B to D). Furthermore, MET blockade by benzamil or curare did not increase mtdTomato signal in mT/mG$^{Tg/+}$;*Tmc1*$^{-/-}$ hair cells, whereas neomycin was still able to induce a detectable increase of mtdTomato fluorescence intensity in these cells (Fig. 4F), agreeing with previously published data showing that PS externalization and membrane blebbing can occur independently in hair cells (*32*). This neomycin-induced increase of mtdTomato signal was not observed in hair cells from mT/mG$^{Tg/+}$;*Tmc1*$^{-/-}$;*Tmc2*$^{-/-}$ (Fig. 3C). In addition to its MET-blocking activity, neomycin is known to bind with high affinity to phosphatidylinositol 4,5-biphosphate (*56*), permeate through functional MET channels, and accumulate inside the hair cell to trigger cell death (*57*). Therefore, permeation

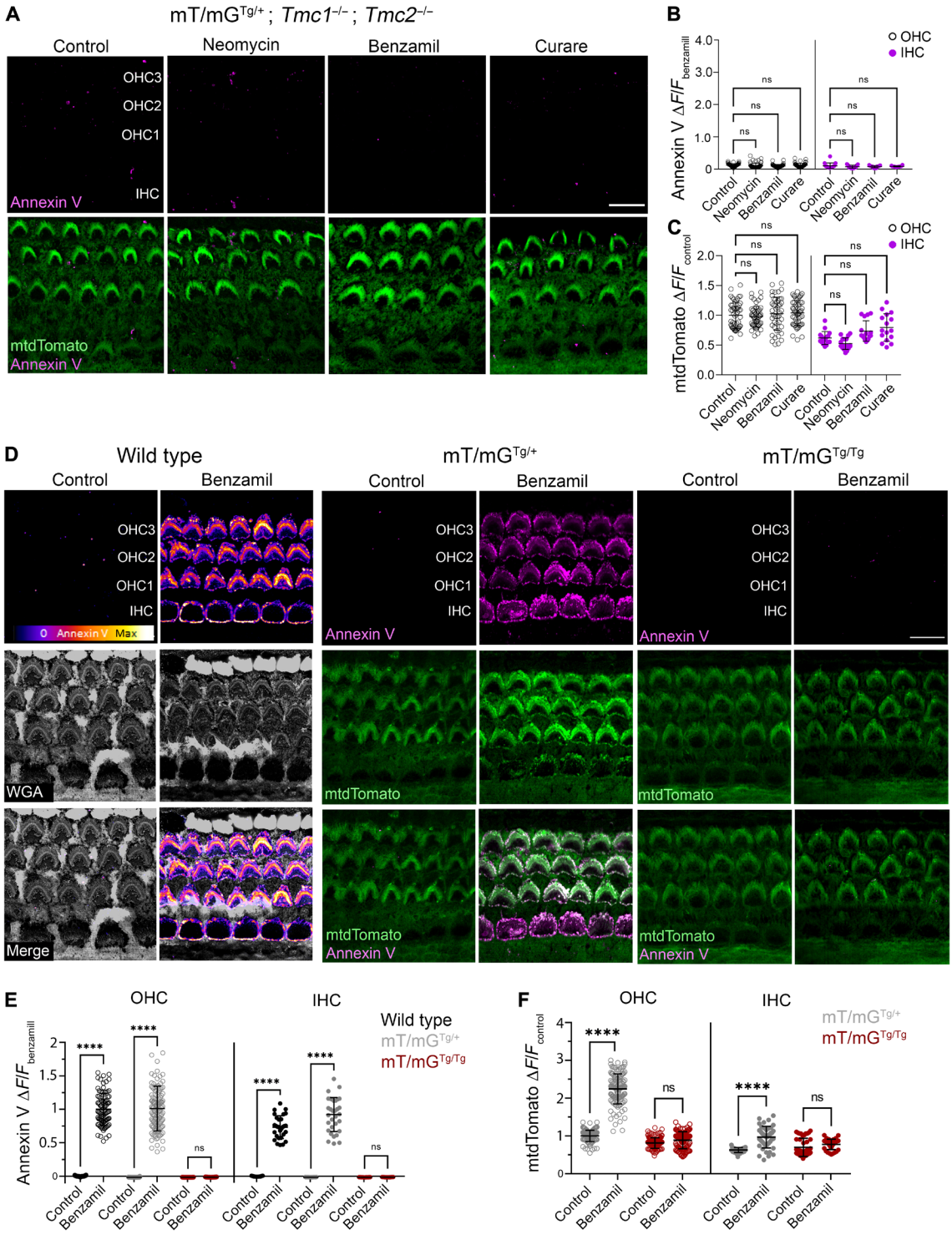

Fig. 3. PS externalization and membrane blebbing in mice lacking MET. (**A**) Confocal images of P6 mT/mG$^{Tg/+}$;*Tmc1*$^{-/-}$;*Tmc2*$^{-/-}$ hair cells incubated with HBSS containing AnV in the absence (control) or presence of 100 μM neomycin, benzamil, or curare. Quantification of the AnV (**B**) and mtdTomato (**C**) fluorescence intensity at the apical region of the OHCs (○) and IHCs (●) treated as in (A). (**D**) Confocal images of hair cells from P6 wild-type, mT/mG$^{Tg/+}$, and mT/mG$^{Tg/Tg}$ littermates incubated in HBSS containing AnV in the absence (control) or presence of 100 μM benzamil. Quantification of the AnV (**E**) and mtdTomato (**F**) fluorescence intensity as in (D). In (B), (C), (E), and (F), mean fluorescence intensity ± SD is represented for $n = 57$ to 126 OHCs and 21 to 43 IHCs from two cochleae. One-way ANOVA analysis was performed (ns $P > 0.05$, and ****$P < 0.0001$). Scale bar, 10 μm. See also fig. S5.

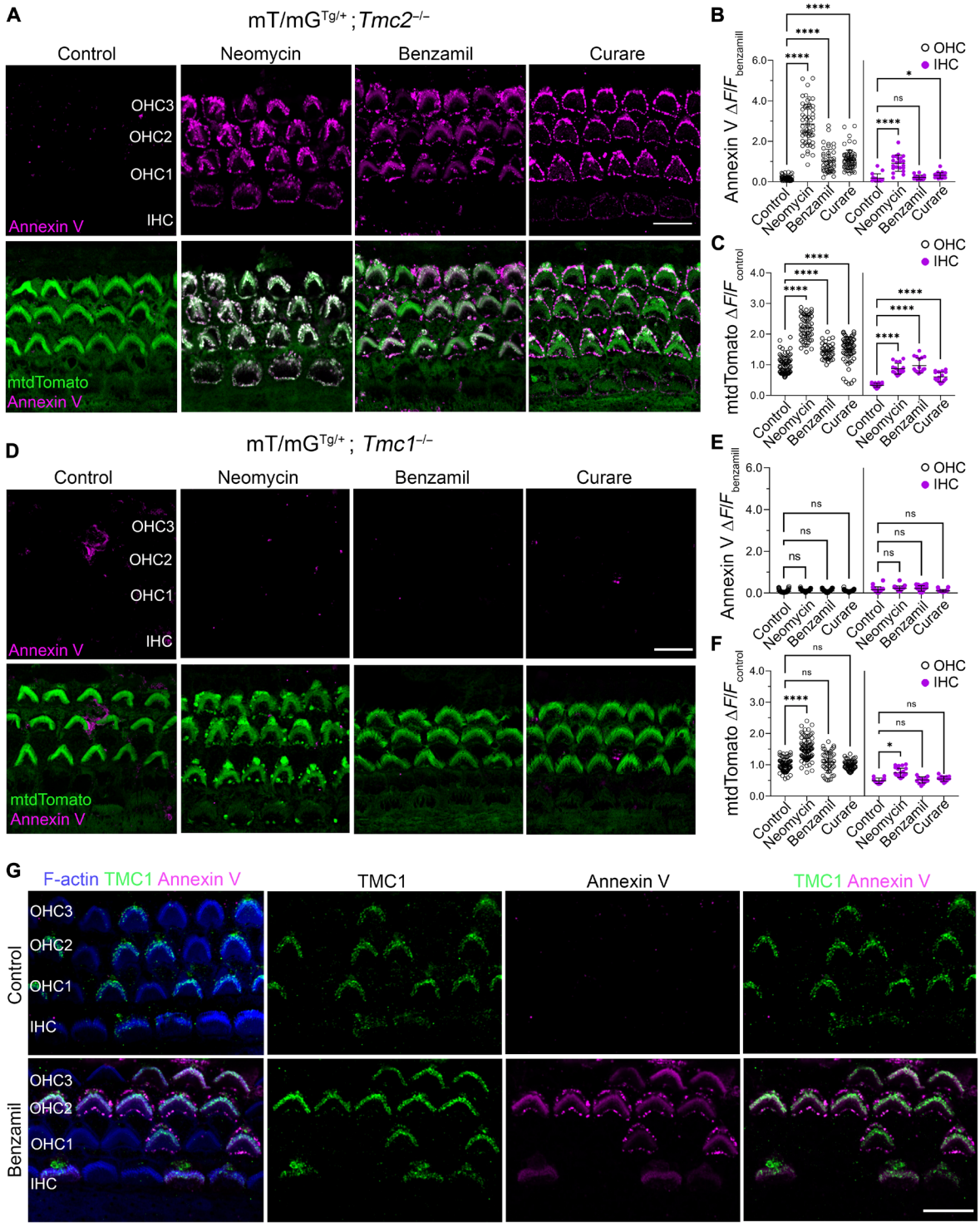

Fig. 4. TMC1, but not TMC2, is required for PS externalization and membrane blebbing. (**A**) Confocal images of P6 mT/mG$^{Tg/+}$;*Tmc2*$^{-/-}$ hair cells incubated with HBSS containing AnV (magenta) in the absence (control) or presence of 100 μM neomycin, benzamil, or curare. Quantification of AnV (**B**) and mtdTomato (**C**) fluorescence intensity at the apical region of OHCs (○) and IHCs (●) treated as in (A). (**D**) Confocal images of P6 mT/mG$^{Tg/+}$;*Tmc1*$^{-/-}$ hair cells treated as in (A). Quantification of AnV (**E**) and mtdTomato (**F**) fluorescence in mT/mG$^{Tg/+}$;*Tmc1*$^{-/-}$ as in (D). (**G**) Confocal images of hair cells from P6 mosaic mice expressing TMC1-cherry untreated (control) or treated with 100 μM benzamil. F-actin (blue) is included to visualize the stereocilia. In (B), (C), (E), and (F), mean ± SD is shown for $n = 45$ to 81 OHCs and 17 to 24 IHCs from two cochleae. One-way ANOVA analysis was performed (ns $P > 0.05$, *$P > 0.05$, and ****$P < 0.0001$). Scale bar, 10 μm. See also fig. S5.

of neomycin through TMC2 MET channels and disruption of the actin-membrane coupling by phosphatidylinositol sequestration (*58*) could explain these results. Together, these data indicate that *Tmc1* is required for PS externalization and membrane blebbing at the apical hair cell region, whereas *Tmc2* is dispensable for regulation of membrane homeostasis following MET channel blockade.

After birth, TMC1 expression in OHCs initiates in the basal portion of the cochlea and progresses toward the apex over the subsequent weeks, following the developmental acquisition of MET and the tonotopic organization of the cochlea (*12*). Consistent with this TMC1 expression gradient of the developing cochlea and with a role of TMC1 in PS externalization, we observed that curare-induced PS externalization in OHCs was stronger in the basal than in the middle cochlear regions, whereas it was undetectable in the apical region of the cochlea from P3 wild-type mice (fig. S6, A to C), when the tonotopic MET gradient differences are still evident (*59*). Similarly, at this age, PS externalization was only detectable in IHCs from the basal region (fig. S6, B and C). Therefore, PS externalization follows the tonotopic gradient of the cochlea. We confirmed that PS externalization was not restricted to the immature auditory system because hair cells from P14 mT/mG$^{Tg/+}$ mice also externalized PS in response to the MET blocker benzamil (fig. S6D).

Having uncovered evidence that TMC1 serves a unique and essential role in regulating membrane homeostasis from experiments where we compared organ of Corti explants obtained from *Tmc1*$^{-/-}$ and *Tmc2*$^{-/-}$ mice, we reasoned that *Tmc1*$^{-/-}$ mice with the *Tmc1*-cherry transgene ectopically inserted into the X chromosome would provide a particularly powerful background to unequivocally establish the privileged role of TMC1 in regulating PS externalization in individual animals. In these female mice with two X chromosomes, roughly half of their hair cells would not express TMC1 because it has been knocked out from chromosome 19 and their wild-type X chromosome is activated, while the other hair cells would express TMC1-cherry because of activation of their X chromosome harboring the ectopic TMC1-cherry (*49*, *60*). Hair cells expressing TMC1-cherry via ectopic insertion into the X chromosome retain functional MET, whereas the others do not (*49*). We therefore crossed *Tmc1*$^{-/-}$ and *Tmc1*-cherry mice to obtain females with mosaic expression of TMC1-cherry in auditory hair cells and used an anti-cherry antibody to identify those cells expressing TMC1-cherry and localize the expression of this transgene at the tips of the two shorter stereocilia rows of OHCs and IHCs (Fig. 4G), consistent with the well-known localization of TMC1 (*49*). Although we could not detect AnV staining in control HBSS-treated cells, indicating that expression of the *Tmc1*-cherry transgene does not alter PS distribution (Fig. 4G), following benzamil treatment we observed robust PS externalization only in TMC1-cherry–expressing hair cells. We conclude from these collective experimental results that TMC1 plays a remarkably unique and essential role in regulating membrane homeostasis in hair cells.

Buffering of intracellular Ca^{2+} triggers PS externalization and membrane blebbing

PS externalization by TMEM16 scramblases is triggered by a rapid rise in intracellular Ca^{2+} concentration (*61*). In contrast, we have demonstrated that PS externalization in hair cells is induced after MET blockade or breakage of the tip link, treatments that have been established to diminish Ca^{2+} influx through the MET channels and decrease intracellular Ca^{2+} (*62*, *63*), thus excluding a role of Ca^{2+}-activated TMEM16 scramblases in the processes studied here. To determine whether a decrease in intracellular Ca^{2+} plays a role in PS externalization, we incubated hair cells from wild-type (fig. S4, F and G) and mT/mG$^{Tg/+}$ mice (Fig. 5) with the membrane-permeable Ca^{2+} chelator, BAPTA-AM, which does not affect the integrity of the tip links or MET (*64*, *65*). As a control, we incubated explants with an equivalent amount of the vehicle used to solubilize BAPTA-AM and observed no detectable AnV staining (Fig. 5 and fig. S4, F and G). In contrast, BAPTA-AM induced robust PS externalization at the apical hair cell region and an increase in mtdTomato fluorescence intensity (Fig. 5), indicating that buffering of intracellular Ca^{2+} is sufficient to trigger PS externalization and membrane blebbing. Like what we observed with MET channel blockers, BAPTA-AM failed to induce PS externalization or an increase of the mtdTomato signal in hair cells from mT/mG$^{Tg/-}$;*Tmc1*$^{-/-}$ mice (Fig. 5, B to D). We therefore conclude that externalization of PS triggered by MET blockade or buffering of intracellular Ca^{2+} both require TMC1.

Tmc1 deafness–causing mutations cause constitutive PS externalization

Next, we investigated the effects of three TMC1 single-point mutations known to cause progressive hearing loss in human and mice with different penetrance. We analyzed PS externalization in hair cells from mice carrying one or two copies of the dominant M412K (also termed Beethoven) or D569N mutations, or the recessive D528N mutation. To qualitatively assess the extent of PS externalization within each *Tmc1* genotype, the AnV signal of untreated hair cells was normalized with the signal of benzamil-treated hair cells for each genotype. However, because M412K and D528N have been reported to alter the MET blockade (*20*, *22*), we cannot directly compare the AnV fluorescence signal between the different mutants and conditions. Unexpectedly, we found that, unlike wild-type hair cells, cells homozygous for any of these three mutations (*Tmc1*$^{M412K/M412K}$, *Tmc1*$^{D569N/D569N}$, and *Tmc1*$^{D528N/D528N}$) showed robust AnV fluorescence signals even in the absence of benzamil (Fig. 6 and fig. S7), indicating that PS externalization at the apical hair cell region of these mutants was constitutive. More notably, this constitutive PS externalization was also detected in untreated hair cells from mice heterozygous for the two dominant TMC1 mutations (*Tmc1*$^{M412K/+}$ and *Tmc1*$^{D569N/+}$; Fig. 6, A and B). In contrast, hair cells carrying just one copy of the recessive D528N mutation (*Tmc1*$^{D528N/+}$) lacked externalized PS and required MET blockade with benzamil to externalize PS (Fig. 6C), like wild-type hair cells. Consistent with our previous results showing that *Tmc2* is dispensable for PS externalization, we also confirmed that differences in the *Tmc2* genotype did not affect constitutive PS externalization in *Tmc1*$^{M412K/+}$ hair cells (Fig. 6, D and E, and fig. S7, A and B). Together, these data demonstrate that these three *Tmc1* deafness–causing mutations alter membrane homeostasis and cause constitutive PS externalization in direct correlation with their deafness phenotypes, leading us to propose that PS externalization could be a critical step in molecular mechanisms of hearing loss.

PS externalization alters TMC1 localization at the stereocilia tips

To explore how this *Tmc1*-dependent PS externalization, membrane blebbing, and ectosome release might cause deafness, we analyzed the TMC1 localization and PS externalization in hair cells as a

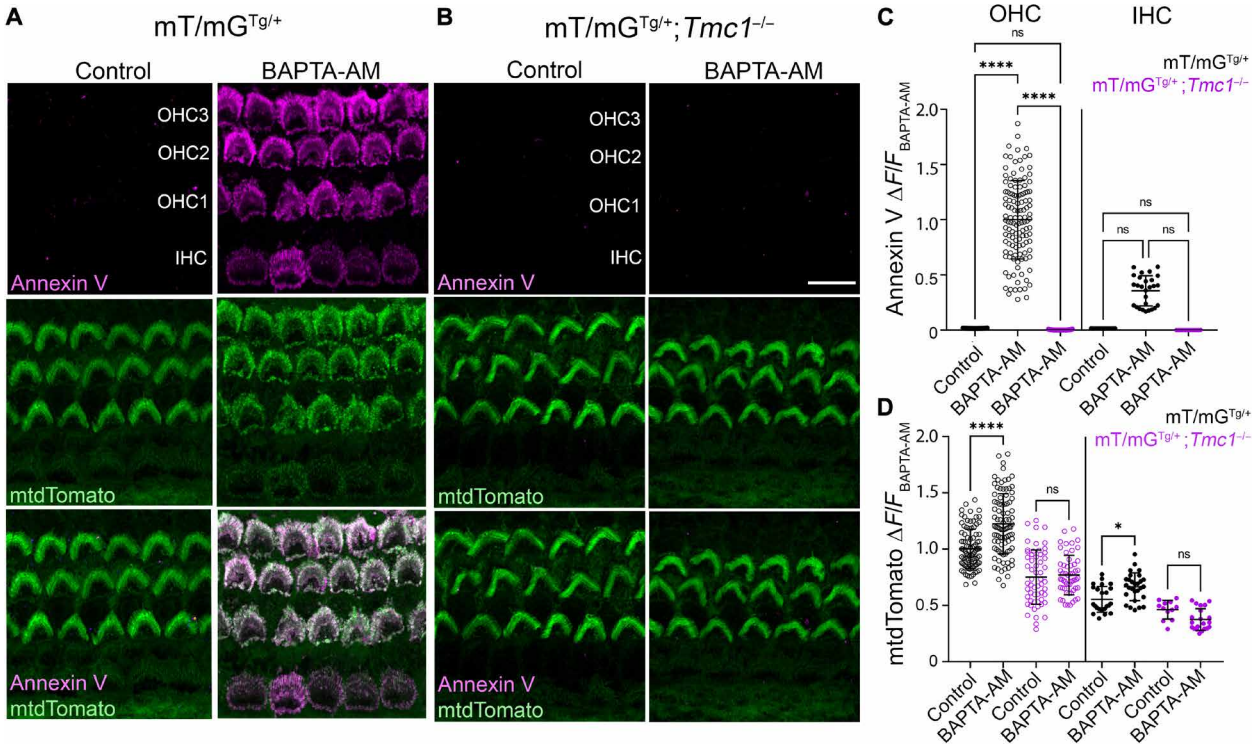

Fig. 5. Buffering of intracellular Ca^{2+} triggers PS externalization and membrane blebbing when TMC1 is present. Confocal images of P6 mT/mG$^{Tg/+}$ (**A**) or mT/mG$^{Tg/+}$;*Tmc1*$^{-/-}$ (**B**) hair cells incubated with HBSS containing AnV (magenta) in the presence of BAPTA-AM or the vehicle (Control). Scale bar, 10 μm. Quantification of AnV (**C**) and mtdTomato (**D**) fluorescence intensity at the apical region of OHCs (○) and IHCs (●) treated as in (A) and (B). Mean fluorescence intensity ± SD is represented for $n = 70$ to 100 OHCs and 15 to 30 IHCs from two cochleae. One-way ANOVA analysis was performed (ns $P > 0.05$, $^*P < 0.05$, and $^{****}P < 0.0001$). See also fig. S4F and G.

function of time following MET blockade with benzamil (Fig. 7). For these experiments, because immunostaining of endogenous TMC1 has proved to be challenging due to its low expression and lack of sensitive and specific antibodies, we used the specific anti-cherry antibody to track the expression of TMC1-cherry in P6 mice expressing the *Tmc1*-cherry transgene in all hair cells (fig. S7B). In the absence of benzamil, TMC1 localized to the tips of the two shorter stereocilia rows in OHCs and IHCs, consistent with previous studies (*49*, *66*), and no externalized PS was detectable by AnV staining (Fig. 7 and fig. S7). However, 10 min after benzamil treatment, we observed externalized PS puncta overlapping with TMC1 at the tips of the shorter stereocilia rows (Fig. 7, A and B, and fig. S7), suggesting that PS initially externalizes near the MET channel. To confirm that PS externalization does not occur at the tips of the longest stereocilia row, we looked at the localization of ESP8, a protein known to be enriched at the longest stereocilia (*67*). However, ESP8 puncta at the tips of the longest stereocilia did not overlap with AnV labeling in P6 IHCs (fig. S7A). Furthermore, we found a strong direct correlation between the AnV and TMC1 fluorescence intensities (fig. S7C), suggesting that the expression level of TMC1 determines the extent of PS externalization. These data suggest that TMC1 is intimately involved in the process of PS externalization.

Later after benzamil treatment, the patterns of PS and TMC1 localization begin to markedly change. After 1 to 2 hours, AnV labeling and TMC1 remained at the stereocilia but TMC1 loses its puncta-like pattern and appears diffuse and enriched in vesicle-like AnV-positive particles at the stereocilia tips and around the cuticular plate (Fig. 7 and fig. S7). After 3 to 4 hours, PS and TMC1 are no longer localized at the stereocilia and instead large AnV- and TMC1-positive vesicle-like particles appeared at the kinocilium site and around the cuticular plate (Fig. 7 and fig. S7). These results suggest that hair cells release TMC1 in PS-positive ectosomes upon activation of PS externalization following MET blockade. Four hours after MET blockade, WGA labeling revealed bulky vesicles at the back of the stereocilia resembling those previously observed by scanning electron microscopy after treatment with ototoxic aminoglycosides (*32*, *33*). The temporal sequence of these observations suggests that blockade of the MET channel triggers the relatively rapid externalization of PS, which is followed more slowly by a process that displaces TMC1 from the stereocilia tips, the cellular localization where TMC1 is required for MET and hearing.

DISCUSSION

The objective of our study was to explore whether the TMC1 and TMC2 proteins that are thought to function as pore-forming subunits of the MET channel also play important roles in regulating membrane homeostasis in mammalian auditory hair cells. Our findings demonstrate that pharmacological blockade of the hair cell MET channel (Fig. 1), tip link disruption (Fig. 2), and intracellular Ca^{2+} buffering (Fig. 5) all trigger PS externalization and membrane remodeling in a TMC1-dependent and TMC2-independent (Fig. 4) manner. Furthermore, we show that mice carrying three distinct *Tmc1* mutations that cause deafness also trigger PS externalization and membrane remodeling (Fig. 6). We show that PS externalization and membrane blebbing also occur after MET blockade in

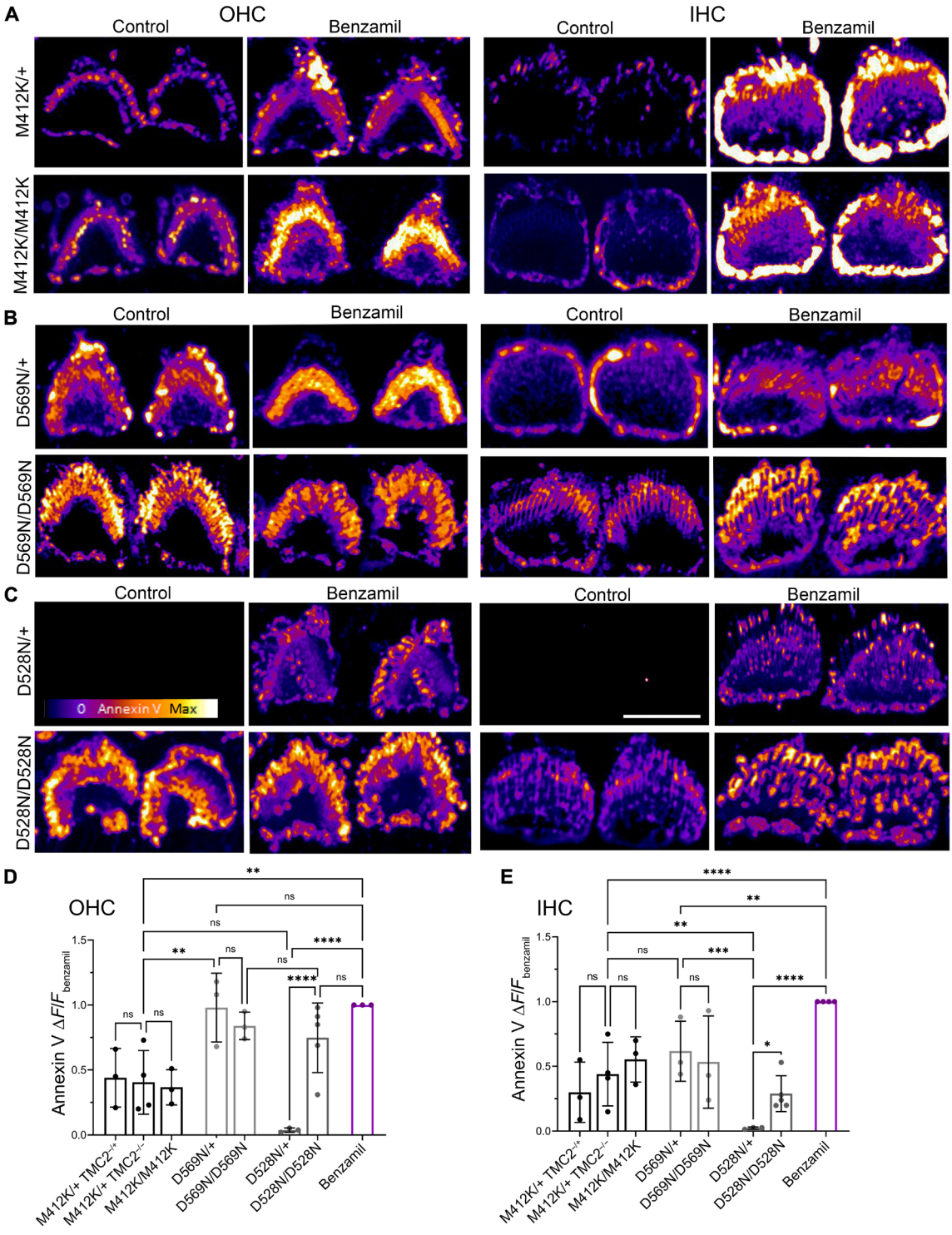

Fig. 6. Constitutive externalization of PS in TMC1 deafness–causing mutant mice. Confocal images of P6 *Tmc1*$^{M412K/+}$ and *Tmc1*$^{M412K/M412K}$ (**A**), *Tmc1*$^{D569N/+}$ and *Tmc1*$^{D569N/D569N}$ (**B**), or *Tmc1*$^{D528N/+}$ and *Tmc1*$^{D528N/D528N}$ (**C**) OHCs and IHCs labeled with AnV in the absence (control) or presence of 100 μM benzamil. Scale bar, 5 μm. Quantification of AnV fluorescence intensity in OHCs (**D**) or IHCs (**E**). Mean ± SD from three to five mice is shown. Each dot represents the mean fluorescence intensity of >100 OHCs or >30 IHCs from one cochlea. One-way ANOVA analysis was performed (ns $P > 0.05$, *$P < 0.05$, **$P < 0.01$, ***$P < 0.001$, and ****$P < 0.0001$). See also fig. S7.

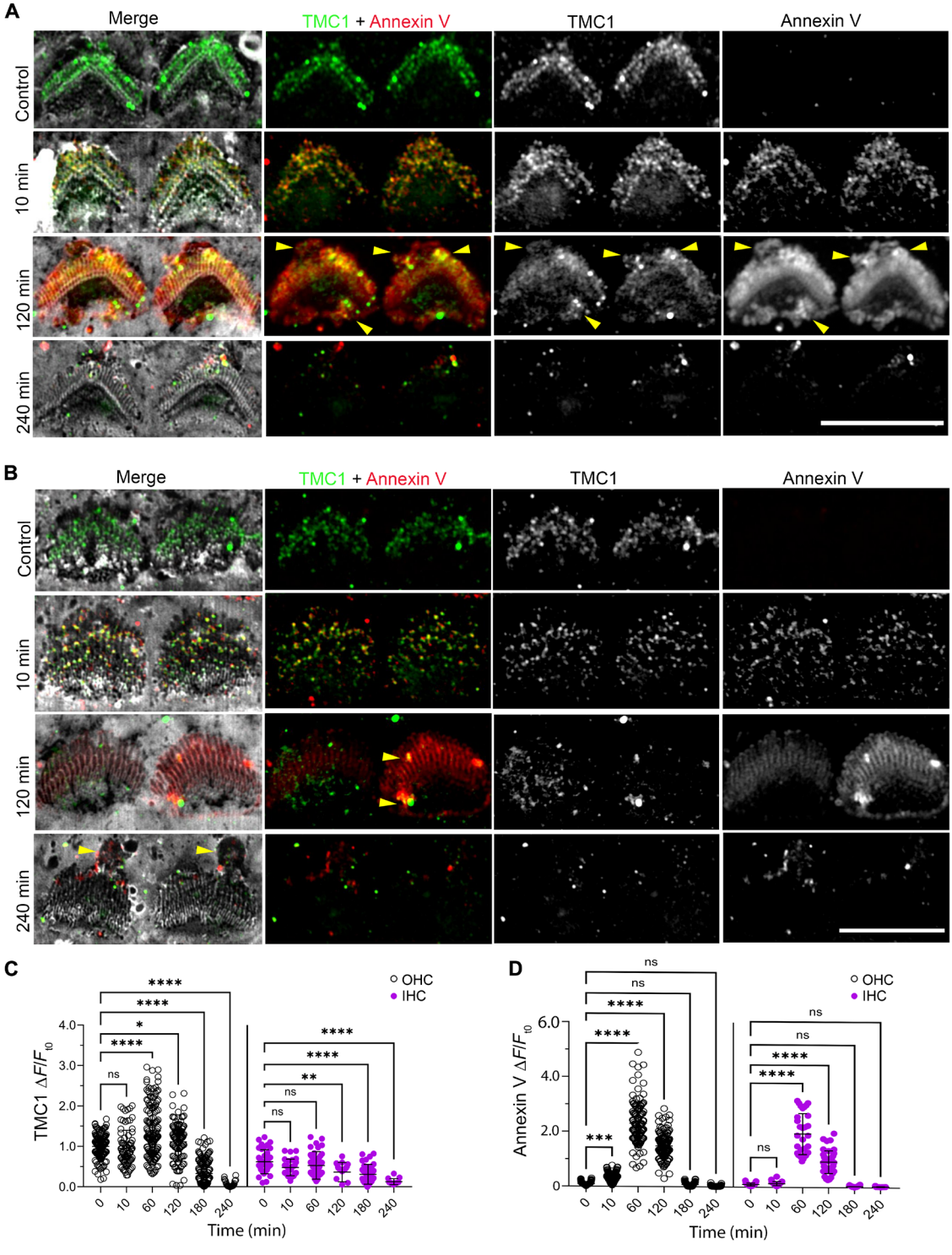

Fig. 7. MET blockage and PS externalization alter TMC1 localization at the stereocilia tips. Confocal images of OHCs (**A**) and IHCs (**B**) from P6 TMC1-cherry mice untreated (control) or treated with 100 μM benzamil for 10, 120, and 240 min. TMC1-cherry (green), AnV (red), and WGA (gray) channels are shown. Scale bar, 5 μm. Yellow arrows indicate protruding TMC1- and AnV-positive vesicles. Quantification of TMC1 (**C**) and AnV (**D**) fluorescence intensity at the apical region of OHCs (○) and IHCs (●) treated as in (A) and (B). Mean ± SD is shown for $n = 79$ to 125 OHCs and 23 to 45 IHCs from two cochleae. One-way ANOVA analysis was performed (ns $P > 0.05$, $^{*}P < 0.05$, $^{**}P < 0.01$, and $^{****}P < 0.0001$). See also fig. S8.

endolymph-like conditions (Fig. 2), highlighting the biological relevance of this process. That this homeostatic mechanism ultimately leads to ectosome release and removal of TMC1 from the stereocilia tips (Fig. 7) implies that a key function of this pathway may be protein and membrane turnover. Overall, our data reveal a previously unknown relationship between TMC1 and hair cell membrane remodeling that is associated with hearing loss.

In the present study, we show that PS externalization in hair cells can be triggered by three distinct classes of MET channel inhibitors: curare, benzamil, and neomycin (Fig. 1). It is important to clarify that although neomycin, like other ototoxic aminoglycosides, is known to permeate through the MET channel, accumulate inside the hair cells, and induce cell death at high concentrations (*68*), the low dose of neomycin and relatively short incubation times used here are not ototoxic (*32*, *69*). Benzamil and curare protect hair cells against aminoglycoside ototoxicity (*70*), yet they both can induce robust PS externalization. Blocker permeation into hair cells is unlikely to be essential for triggering PS externalization because curare is a nonpermeant blocker of the MET channel (*43*) and robust externalization can be triggered by breakage of the tip links required for MET (Fig. 2). Therefore, although we cannot exclude that these drugs may have multiple distinct actions on hair cells, it seems reasonable to conclude that the hair cell–specific PS externalization observed in our experiments is not a consequence of cell death or permeation of the drugs inside the hair cells, but most likely due to inhibition of MET channels, a function common to all three molecules. Because the MET channel is Ca^{2+} permeable and inhibition of the MET channel or breakage of the tip links has been established to lower intracellular Ca^{2+} (*48*, *63*, *71*), we investigated the effects of a membrane-permeant Ca^{2+} chelator and found that this manipulation is sufficient to trigger PS externalization (Fig. 5). Although we have not directly measured intracellular Ca^{2+} concentrations in our study, we propose that lowering of intracellular Ca^{2+} is the common trigger for PS externalization when activity of the MET channel is disrupted. PS externalization and membrane blebbing are more robust in OHCs than in IHCs under our experimental conditions. Although the molecular mechanisms of this difference will require further investigation, differences in the OHC and IHC membrane composition (*72*), Ca^{2+} homeostatic mechanisms (*73*), resting open probability of the MET channel (*74*), and TMC1 expression levels (*66*) might explain the less robust PS externalization observed in IHCs.

One major finding of our study is that PS externalization and membrane blebbing require expression of *Tmc1*, but not *Tmc2* (Fig. 4). While both *Tmc1* and *Tmc2* can restore MET in young animals, the unique role of TMC1 in regulating membrane homeostasis identified by our study may explain why TMC1 plays a more important role than TMC2 in hearing. $Tmc1^{-/-}$ mice are deaf, $Tmc2^{-/-}$ mice are phenotypically normal, and $Tmc1^{-/-}$;$Tmc2^{-/-}$ mice are deaf and present vestibular dysfunction, indicating that *Tmc1* can compensate for the lack of *Tmc2* in the vestibular and auditory systems, but that *Tmc2* cannot compensate for the lack of *Tmc1* in the auditory system (*12*–*14*). Here, we identify a key functional difference between TMC1 and TMC2 that could explain the different requirement for these two proteins in hearing and balance. Unlike vestibular hair cells, auditory hair cells are tonotopically organized along the cochlea and tuned to sense and amplify precise frequencies (*59*). We provide evidence that PS externalization is directly related to TMC1, whose expression levels follow the tonotopic gradient of the cochlea (*66*). While our study focused on PS externalization, loss of the membrane asymmetry also causes changes in membrane thickness and externalization of other phospholipids such as phosphatidylinositols, known to regulate MET adaptation (*75*, *76*). The ability of TMC1 to remodel the membrane and alter the lipid distribution may equip TMC1 channels to respond and adapt to different frequencies. Accordingly, TMC1 channels show faster adaptation than TMC2, and the TMC1 M412K and D569N deafness-causing mutations affect MET adaptation (*5*, *22*, *77*). Although the temporal resolution or our experiments is limited to the time scale of minutes, it will be fascinating to explore more rapid molecular events involved in the process by which TMC1 MET channels alter membrane homeostasis.

In mammalian cells, PS exposure on the extracellular leaflet of the plasma membrane is the result of the action of lipid scramblases (*28*). In recent years, notable progress has been made in understanding the biological relevance of lipid scrambling and the proteins that have this activity (*47*, *61*, *78*–*82*), but its physiological role in hair cells and hearing remains unexplored. Although hair cells express known lipid scramblases (*83*, *84*), the PS externalization we observed in hair cells is TMC1-dependent and can be triggered by lowering intracellular Ca^{2+}, suggesting that the PS externalization is unlikely to be mediated by Ca^{2+}-activated TMEM16s (*79*), caspase-activated XK-related protein 8 (*78*), or constitutively activated scramblases such as class A G protein–coupled receptors (*82*) or the intracellular TMEM41B, VMP1 (*80*), and Atg9 (*85*) lipid scramblases. Instead, given the known structural relationship between TMC1 and TMEM16 scramblases, the finding that $Tmc1^{-/-}$ hair cells fail to externalize PS, and the discovery that three different *Tmc1* deafness mutations cause constitutive PS externalization, we speculate that in addition to forming the pore of the MET channel, TMC1 might moonlight as a Ca^{2+}-inhibited lipid scramblase.

As buffering intracellular Ca^{2+} is sufficient to trigger PS externalization in wild-type hair cells and all three *Tmc1* mutations studied here (M412K, D569N, and D528N) have been shown to reduce the Ca^{2+} permeability of MET channels (*5*, *17*, *19*, *20*, *22*), it is intriguing to consider whether this alteration in Ca^{2+} permeability might be sufficient to trigger PS externalization in the mutants. For the recessive D528N mutant, one copy of the mutant diminishes Ca^{2+} permeability by about twofold and two copies of the mutation diminish Ca^{2+} permeability by about sevenfold in OHCs (*20*), raising the possibility that alterations in Ca^{2+} permeability might be sufficient to explain why the mutant triggers PS externalization. However, for the two dominant mutations (M412K and D569N), one copy of each mutant diminishes Ca^{2+} permeability by 1.8- to 2.2-fold, yet two copies of the mutations diminish Ca^{2+} permeability by only 2.8- to 3.4-fold in OHCs (*17*, *19*, *22*), suggesting that changes in Ca^{2+} permeability alone cannot explain the pattern of constitutive PS externalization observed here (Fig. 6). Thus, it seems likely that the two dominant mutations trigger constitutive PS externalization by a mechanism distinct from their effects on Ca^{2+} permeability of the MET channel.

Alterations in the functional properties of MET channels measured in neonatal mice have been described for several *Tmc1* mutations that ultimately cause hearing loss (*5*, *17*, *19*–*22*, *77*, *86*), which can only be accurately measured in older animals where hair cells from *Tmc1* deafness–causing mutants and $Tmc1^{-/-}$ mice have begun to die (*18*–*21*). Thus, it remains unclear whether alterations in the MET channel properties per se are sufficient to cause hearing loss or whether the subsequent hair cell death is ultimately

responsible for deafness. The MET channel properties are clearly impaired in *Tmc1*$^{D528N/+}$ hair cells, but these cells do not degenerate, and *Tmc1*$^{D528N/+}$ mice have normal hearing (*20*), providing one clear example where altered MET channel properties do not cause loss of hair cells or deafness. It has therefore been proposed that TMC1 may play other roles that are critical for hair cell survival (*19*, *20*, *22*). Our discovery that *Tmc1* regulates membrane homeostasis and *Tmc1* deafness–causing mutations trigger constitutive PS externalization raises the possibility that hair cell membrane homeostasis is essential for hair cell survival and hearing. Mutations in the stereocilia ATP8B1 flippase that transports PS from the outer to the inner membrane leaflet causes hair cell death and hearing loss (*87*), consistent with an important role for membrane homeostasis in hair cell death. Moreover, PS is constitutively externalized in hair cells from heterozygotic and homozygotic mice carrying the autosomal dominant M412K and D569N mutations, but only in homozygotic mice carrying the recessive D528N mutation (Fig. 6), providing a clear correlation between PS externalization and deafness phenotype in these mice and supporting a role of altered membrane homeostasis in hair cell death and deafness.

Upon MET blockade, we observed that PS externalization, membrane blebbing, and ectosome release ultimately lead to the loss of TMC1 from the hair cell bundle (Fig. 7), suggesting that a key function of this TMC1-dependent membrane remodeling mechanism may be protein turnover to restore functional MET once it has been disrupted. Consistent with this hypothesis, the transducing stereocilia tips of *Tmc1*$^{-/-}$ hair cells have been shown to display accumulation of TMC2 and altered protein distribution (*66*, *88*). Loss of TMC1 channels would explain the protective effect described for several blockers of the MET channel against ototoxic compounds (*89*). In the case of *Tmc1* mutant hair cells, constitutive PS externalization in these hair cells may lead to continued loss of TMC1 from the

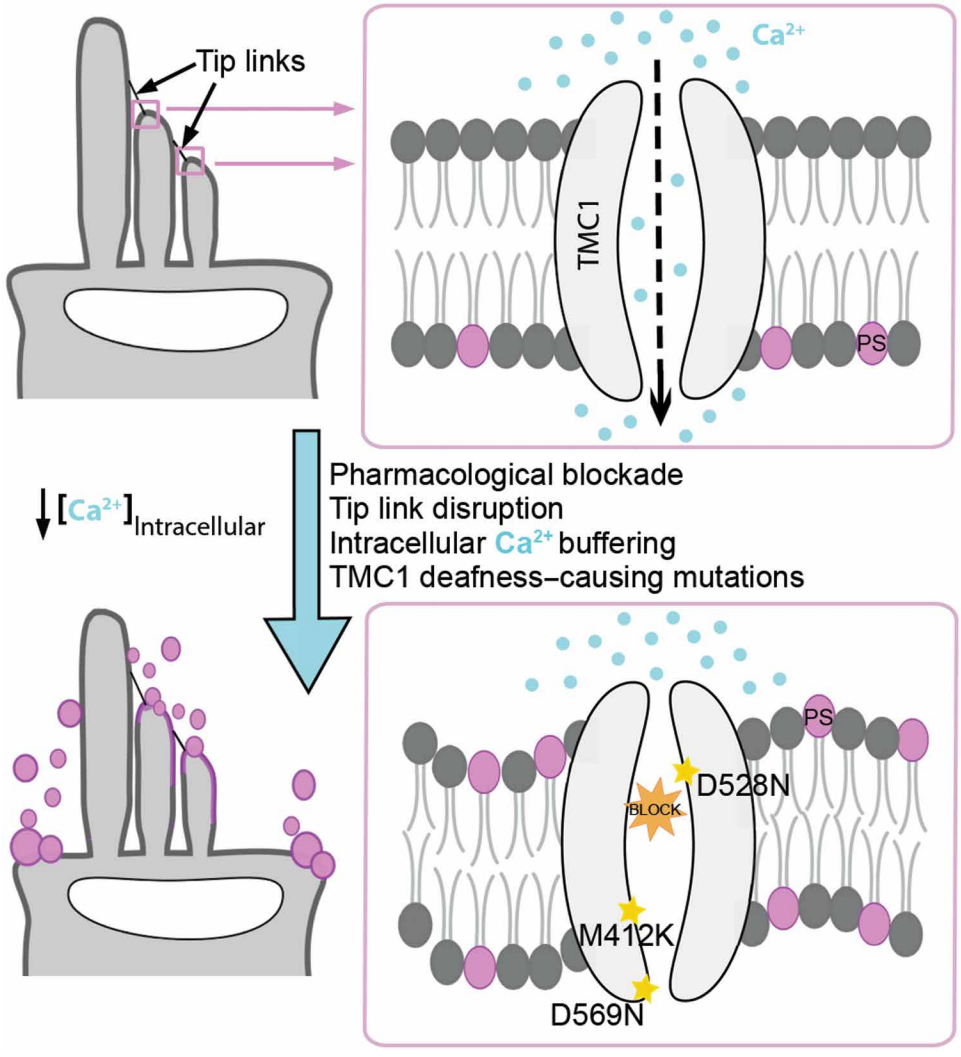

Fig. 8. TMC1-dependent regulation of the apical hair cell membrane homeostasis. Plasma membrane asymmetry is preserved in wild-type murine auditory hair cells under physiological conditions. However, pharmacological blockade of the MET channel, disruption of the tip links, or intracellular Ca^{2+} buffering triggers the externalization of PS and membrane blebbing at the stereocilia and apical region of hair cells expressing TMC1. In addition, two autosomal dominant (M412K and D569N) and one recessive (D528N) *Tmc1* deafness–causing mutations cause constitutive externalization of PS that correlates with deafness phenotype in these mutant mice, highlighting the relevance of membrane homeostasis in hearing.

hair cell bundle, which could explain the coincidental degeneration and loss of hair cells reported in *Tmc1*$^{-/-}$ and *Tmc1* M412K, D569N, and D528N mutant mice (*12*, *18*–*20*). Overall, our findings suggest that stereocilia might use membrane remodeling and ectosome release as a mechanism to regulate membrane and protein homeostasis, resembling cilia (*90*).

In conclusion, our study reveals new insights into the importance of membrane homeostasis in hair cells for both MET and hearing. We show that TMC1 is essential for the externalization of PS and membrane blebbing at the apical hair cell membrane triggered by blockade of the MET channels, disruption of the tip links, or buffering of the intracellular Ca^{2+} (Fig. 8). Furthermore, three TMC1 deafness–causing mutations cause constitutive PS externalization matching their hearing-loss phenotype and suggesting that loss of hair cell plasma membrane asymmetry may be a mechanism of hair cell loss and deafness. The discovery of a TMC1-dependent autoregulatory process opens new avenues of research to understand the mechanisms of hair cell bundle development, stereocilia remodeling, and deafness.

MATERIALS AND METHODS

Mouse strains

Wild-type C57BL/6J (strain 000664) and mT/mG mice (strain 007676) were purchased from The Jackson Laboratory and breed in our animal facility to obtain the desired phenotypes. *Tmc1*$^{-/-}$, *Tmc2*$^{-/-}$ (RRIDs: IMSR_JAX:019146 and IMSR_JAX:019147) (*12*) and transgenic mice endogenously expressing TMC1 fused at the C-terminal to Cherry fluorescent protein in a *Tmc1*$^{-/-}$;*Tmc2*$^{-/-}$ background (TMC1-cherry, RRID: IMSR_JAX:028392) (*49*) were obtained from A. Griffith (National Institute on Deafness and Other Communication Disorders). *Tmc1*$^{-/-}$, *Tmc2*$^{-/-}$ mice were crossbreed with mT/mG$^{Tg/Tg}$ mice to obtain double (mT/mG$^{Tg/Tg}$;*Tmc1*$^{-/-}$ or mT/mG$^{Tg/TG}$;*Tmc2*$^{-/-}$) and triple (mT/mG$^{Tg/Tg}$;*Tmc1*$^{-/-}$;*Tmc2*$^{-/-}$) transgenic mice. Because only heterozygous mice for the mtdTomato transgene (mT/mG$^{Tg/+}$) were used in our experiments (except where indicated), mT/mG$^{Tg/Tg}$ and *Tmc1*$^{-/-}$ mice were crossbred with *Tmc1*$^{-/-}$ to obtain heterozygous mT/mG$^{Tg/+}$;*Tmc1*$^{-/-}$ mice. The same protocol was followed to generate mT/mG$^{Tg/+}$;*Tmc2*$^{-/-}$ and mT/mG$^{Tg/+}$;*Tmc1*$^{-/-}$;*Tmc2*$^{-/-}$ mice. *Tmc1*$^{M412K/M412K}$, *Tmc1*$^{D569N/D569N}$, and *Tmc1* $^{D528N/D528N}$ mice were bred with wild type to obtain heterozygous mice. For all genotypes, a mixture of male and female mice was used. Mice were kept on a 12-hour light/dark cycle and were allowed solid food and water ad libitum. The animal care and experimental procedures were performed following the *Guide for the Care and Use of Laboratory Animals*. They were approved by the Animal Care and Use Committee of the National Institute of Neurological Disorders and Stroke (Animal protocol number 1336).

Genomic DNA extraction from tail snips and genotyping polymerase chain reactions (PCRs) were performed using a MyTaq Extract-PCR kit (Bioline, Taunton, MA). All the mice were genotyped by the fragment PCR method using the primers listed in table S1 and as indicated in The Jackson Laboratory website or previously described (*23*). PCR products were run on 2% agarose gels, and the Quick-Load 100 bp DNA Ladder (New England Biolabs) was used for fragment size visualization. The PCR fragments obtained from genotyping of the *Tmc1* M412K mice were purified and sent for sequencing, whereas the PCR fragments from the *Tmc1* D569N or D528N mice were further digested with Eco RI or Acl I, respectively.

Dissection of inner ear tissue and sample preparation for imaging

Excision of the inner ear from P6 wild-type C57BL/6J, reporter mT/mG, or *Tmc* mutant mice and further cochleae dissection, including removing the semicircular canals and vestibular organs, were performed in cold Leibovitz's L15 medium. Cochlear tissues were placed on a Corning PYREX 9 depression plate well HBSS to remove the cochlear bone and expose the organ of Corti. At least three cochleae from littermate mice were used for each experimental condition. Drug treatments were performed at this stage. The cochlear tissues were incubated with the indicated drugs and fluorescent dyes for 25 min at room temperature (RT) in an orbital shaker and protected from light. Without mechanical stimulation, a population of MET channels will be open at rest because of tension on the channel by the tip links (*36*), but we performed our experiments under gentle shaking conditions to increase the open probability of the MET channel. After treatment, tissues were washed twice with HBSS and fixed in 4% paraformaldehyde (PFA) in HBSS for 30 min. Fixed tissue was washed with HBSS to remove PFA, and the spiral ligament and the tectorial membrane were removed to obtain fixed organ of Corti explants in HBSS buffer. Tissue was washed with phosphate-buffered saline (PBS) to remove salt and finally mounted with ProLong Diamond antifade mounting medium (Thermo Fisher Scientific) on a Superfrost plus microscope slide (Fisherbrand) and covered with a #1.5 glass coverslips of 0.17 ± 0.02 mm thickness (Warner Instruments) for confocal imaging.

Blockage of the MET channel

Dissected organ of Corti from wild-type C57BL/6J, mT/mG$^{Tg/+}$, or *Tmc1* or *Tmc2* single- and double-knockout littermate mice were incubated in HBSS containing 1:25 AnV–Alexa Fluor 647 (Thermo Fisher Scientific) and CF488A-WGA (20 μg/ml; Biotium) in the absence (control) or presence of neomycin, benzamil at 0.1 mM, or curare at 0.1 mM and 1 mM concentration. A stock solution of 30 mM benzamil hydrochloride hydrate (Sigma-Aldrich) was prepared in dimethyl sulfoxide (DMSO). Neomycin trisulfate salt hydrate (Sigma-Aldrich) was dissolved at 50 mM in water. Tubocurarine hydrochloride pentahydrate (Curare, Sigma-Aldrich) was dissolved at 50 mM in water. Stock solutions were aliquoted and stored at −30°C. AnV was used to detect and visualize the externalized PS because of its ability to bind PS with high affinity in a Ca^{2+}-dependent manner (*40*). WGA binds to oligosaccharides and has been shown to label the surface of both IHCs and OHCs without blocking transduction (*41*, *91*). Under all the conditions we tested, WGA labeled the stereocilia and hair cell surface and was also accumulated at the surface of pillar and Hensen cells (Fig. 1A). P6 heterozygous mT/mG mice (mT/mG$^{Tg/+}$), which express a membrane-targeted tandem dimer tomato (mtdTomato) fluorescent protein and preserve MET (*42*), were used to visualize the stereocilia and hair cell membrane. Cochlear tissues were incubated with the drugs and fluorescent dyes for 25 min at RT in an orbital shaker protected from light. After treatment, tissues were washed twice with HBSS, fixed in 4% PFA in HBSS for 30 min, and prepared for imaging as described above. P6 littermate mice obtained from mT/mG$^{Tg/+}$ and mT/mG$^{Tg/+}$ breeding were used in the experiments comparing wild-type, mT/mG$^{Tg/+}$, and mT/mG$^{Tg/Tg}$ hair cells. One cochlea was incubated in HBSS, and the other one was treated with benzamil. Cochleae from wild-type or *Tmc2*$^{-/-}$ mice

were included in the experiments, with *Tmc1*$^{-/-}$ and *Tmc1*$^{-/-}$;*Tmc2*$^{-/-}$ mice as positive controls.

For live imaging experiments, dissected organs of Corti from P4-P6 wild-type mice were cultured over collagen-covered 35-mm glass-bottom cell culture dish with 2 ml of Leibovitz's L15 medium with fetal bovine serum (FBS) at 37°C and 5% CO_2. After 2- to 4-hour incubation, 5 μl of CellMask Green plasma membrane stain (Thermo Fisher Scientific) was added to the Leibovitz's L15 medium with FBS and incubated at 37°C for 5 to 10 min. Cell medium was removed, and 1:50 AnV was added in Leibovitz's L15 medium without FBS. After collecting some images of time cero, 100 μM curare was added to the AnV-containing medium, and imaging acquisition was resumed at RT. An equivalent amount of water was added to the control samples.

Disruption of the tip links with BAPTA

We incubated organ of Corti explants with 5 mM BAPTA in HBSS without Ca^{2+} and Mg^{2+} (HBSS-CFM) containing CF488A-WGA at 20 μg/ml for 25 min. A stock of BAPTA tetrapotassium salt (Thermo Fisher Scientific) was dissolved at 50 mM in water, aliquoted, and stored at −30°C. Organ of Corti explants were incubated in HBSS or HBSS-CFM buffer containing CF488A-WGA at 20 μg/ml as controls. Tissue explants were then washed once with HBSS, and AnV–Alexa Fluor 647 (Thermo Fisher Scientific) was added at a 1:25 dilution in HBSS for 5 min. Tissues were washed twice with HBSS to remove the excess of AnV, fixed in 4% PFA in HBSS for 30 min, and prepared for imaging as described above. In addition, experiments with the C2 domain of lactadherin fused to a fluorescent clover protein (clover-Lact-C2) were performed to detect the externalized PS in the absence of Ca^{2+}. In these experiments, excised organs of Corti tissues were incubated in HBSS-CFM with CF488A-WGA (20 μg/ml) and clover-Lact-C2 (3 μg/ml) for 25 min at RT under gentle shaking. Tissues were then washed twice with HBSS to remove the excess of WGA and clover-Lact-C2, fixed in 4% PFA in HBSS for 20 min, and prepared for imaging as described above.

Expression and purification of clover-Lact-C2

A cDNA construct consisting of Clover fluorescent protein followed by a hexa-histidine tag and lactadherin-C2 [Clover-(His)6-LactC2] in the pET-28 bacterial expression vector together with pLysSRARE2 plasmid [both shared by L. Chernomordik, National Institute of Child Health and Human Development (NICHD)] were electroporated into ClearColi BL21(DE3) according to the manufacturer's protocol (Lucigen). Bacterial colonies that grew in an LB plate containing kanamycin (100 μg/ml) and chloramphenicol (30 μg/ml) were considered positive for incorporating both plasmids and selected for protein expression. Cells were grown in 0.5 liters of LB Miller medium at 37°C in kanamycin (100 μg/ml) and chloramphenicol (30 μg/ml) until the culture reached A_{600} = 1. After the addition of 1 mM IPTG (isopropyl-β-D-thiogalactopyranoside), the culture was grown for 3 hours at 37°C. Next, cells were lysed in B-PER bacterial protein extraction reagent (Thermo Fisher Scientific) containing 2500 U of deoxyribonuclease I (Sigma-Aldrich), 0.1 mM phenylmethylsulfonyl fluoride, and SIGMAFAST EDTA-free protease inhibitor cocktail (Sigma-Aldrich). After centrifugation at 20,000*g* for 20 min, Clover-(His)6-LactC2 was purified from the supernatant with 3 ml of the TALON superflow metal affinity resin (Clontech). The resin was washed with 5 mM imidazole in PBS, and the protein was eluted with 100 mM imidazole in PBS (fig. S4C). The eluted protein was dialyzed against PBS and concentrated to a final concentration of 1.036 mg/ml.

Perilymph and endolymph-like buffers

The perilymph-like buffer used in our experiments had a composition of 125 mM NaCl, 1.3 mM $CaCl_2$, 3.5 mM KCl, 1.5 mM $MgCl_2$, 10 mM Hepes (pH 7.4), and 5 mM glucose, and the osmolarity was adjusted to 290 mOsm with NaCl. The composition of the endolymph-like buffer used was 1 mM NaCl, 0.025 mM $CaCl_2$, 126 mM KCl, 0.025 mM $MgCl_2$, 10 mM Hepes (pH 7.4), and 0.5 mM glucose, and the osmolarity was adjusted to 315 mOsm with KCl. Cochlear tissues from P6 mT/mG$^{Tg/+}$ mice were dissected to remove the cochlear bone and expose the organ of Corti. Organ of Corti explants were incubated in perilymph-like or endolymph-like buffer with benzamil or the equivalent volume of DMSO (control) for 25 min at RT with gentle shaking in an orbital shaker protected from light. Tissue explants were then washed once with HBSS, and AnV–Alexa Fluor 647 was added at a 1:25 dilution in HBSS for 5 min to all the samples. Tissues were washed twice with HBSS to remove the excess of AnV, fixed in 4% PFA in HBSS for 30 min, and prepared for imaging as described above.

Buffering of intracellular Ca^{2+}

To buffer the intracellular Ca^{2+} concentration in murine hair cells, we use the Ca^{2+} quelator BAPTA-AM. BAPTA-AM is an acetoxymethyl (AM) ester derivative of BAPTA that binds Ca^{2+} only after its AM group is removed by cytoplasmic esterases. Treatment of cochlear tissue with BAPTA-AM does not affect the integrity of the tip links or does not alter the resting probability of the MET channel (*64*, *65*). A stock of cell-permeant BAPTA-AM (Invitrogen) was prepared at 20 mM in 20% pluronic F-127 in DMSO, aliquoted, and stored at −30°C. Pluronic F-127 is a mild non-ionic detergent useful for solubilizing BAPTA-AM and facilitating AM esters loading into cells. A stock solution of HBSS containing CF488A-WGA (20 μg/ml) and AnV at a 1:25 dilution was prepared and split into two tubes. BAPTA-AM (20 mM) in 20% pluronic F-127 in DMSO was added at a final concentration of 20 μM, while an equivalent volume of the vehicle (20% pluronic F-127 in DMSO) was added to the other tube and used as a control in these experiments. Dissected organ of Corti explants were incubated with the solution containing BAPTA-AM or the vehicle and incubated for 25 min at RT under gentle shaking. After the incubation, the tissue was washed a couple of times with HBSS, fixed with 4% PFA, and prepared for imaging.

TMC1-cherry immunostaining and time course

Organ of Corti explants from TMC1-cherry mice were dissected as described above. Tissue explants were then incubated with HBSS (control) or HBSS with 100 μM benzamil in the presence of 1:25 AnV–Alexa Fluor 647 and CF488A-WGA (20 μg/ml). Ten, 60, 120, 180, and 240 min after benzamil addition, tissues were washed twice with HBSS and fixed in 4% PFA in HBSS for 30 min. Fixed tissues were washed with HBSS to remove PFA, and the spiral ligament and the tectorial membrane were removed to obtain fixed organ of Corti explants in HBSS buffer. To label TMC1-cherry, tissues were permeabilized in 0.5% Triton X-100 in PBS for 20 min. Tissues were washed twice with PBS for 5 min to remove the excess of Triton X-100 and then blocked for 1 hour at RT with blocking buffer (PBS containing 10% goat serum and 5% bovine serum albumin). The primary antibody anti–red fluorescent protein (660-401-379,

Rockland) was added at 1:100 in blocking buffer and incubated at 4°C overnight in an orbital shaker with gentle shaking protected from light. The next morning, tissues were washed three times with PBS to remove the excess of primary antibody. Goat anti-rabbit secondary antibody conjugated with Alexa Fluor 594 (R37117, Molecular Probes) at the manufacturer's recommended concentration and 1:100 CF405M phalloidin (Biotium) in blocking buffer were added to the tissue and incubated for 30 min at RT. Tissues were then washed two to three times with PBS and prepared for imaging as described above.

PS externalization in TMC1 mutants

To compare the AnV fluorescence in the *Tmc1* mutant mice, we incubated one cochlea in HBSS containing AnV–Alexa Fluor 647 at a 1:25 dilution and CF488A-WGA (Biotium) at 20 μg/ml and the other cochlea in the same buffer supplemented with 100 μM benzamil for 25 min at RT in an orbital shaker protected from light. After treatment, tissues were washed twice with HBSS, fixed in 4% PFA in HBSS for 30 min, and prepared for imaging as described below.

Quantification and statistical analysis

Super-resolution imaging was performed in the Microscopy and Imaging Core (NICHD) with a confocal laser scanning microscope (Zeiss LSM 880, Carl Zeiss AG) equipped with a 32-channel Airyscan detector. Images of the whole organ of Corti were taken with a 20× objective (Carl Zeiss). To image the hair cells, we used oil immersion alpha Plan-Apochromat 63×/1.4 Oil Corr M27 objective (Carl Zeiss) and immersol 518F medium [ne = 1.518 (30°)]. A z-stack of images from the stereocilia to the apical half of the hair cell body was collected with identical image acquisition settings, no averaging, and optimal parameters for x, y, and z resolution for each independent experiment. Image acquisition and Airyscan image processing were performed with Zen Black 2.3 SP1 software (Carl Zeiss) using the Airyscan three-dimensional reconstruction algorithm with the automatic default Wiener filter settings. Samples from each experiment, including control and treated or wild-type and mutant mice, were imaged on the same day to limit variability.

Microscopy data analysis and quantification were done in ImageJ. To measure the fluorescence intensity at the apical region of the hair cells, we generated a region of interest (ROI) around each OHCs and IHCs using the elliptical tool as depicted in Fig. 1A. The fluorescence intensity of an equivalent ROI in an area outside the hair cells was considered as background and subtracted from the values at the hair cells for each image. AnV and mtdTomato fluorescence intensities were quantified in each hair cell. mtdTomato fluorescence intensity was normalized against the mtdTomato fluorescence intensity of the control samples, whereas AnV fluorescence intensity was normalized against the fluorescence of the treated samples as indicated in the corresponding y axis. The number of cells and tissues analyzed in each condition and the statistical method used are indicated in the figure legends. GraphPad Prism V.7 software was used to generate the graphs and perform the statistical analysis.

SUPPLEMENTARY MATERIALS

Supplementary material for this article is available at https://science.org/doi/10.1126/sciadv.abm5550

View/request a protocol for this paper from *Bio-protocol*.

REFERENCES AND NOTES

1. R. Fettiplace, K. X. Kim, The physiology of mechanoelectrical transduction channels in hearing. *Physiol. Rev.* **94**, 951–986 (2014).
2. J. A. Assad, G. M. Shepherd, D. P. Corey, Tip-link integrity and mechanical transduction in vertebrate hair cells. *Neuron* **7**, 985–994 (1991).
3. A. J. Hudspeth, D. P. Corey, Sensitivity, polarity, and conductance change in the response of vertebrate hair cells to controlled mechanical stimuli. *Proc. Natl. Acad. Sci. U.S.A.* **74**, 2407–2411 (1977).
4. B. Pan, N. Akyuz, X. P. Liu, Y. Asai, C. Nist-Lund, K. Kurima, B. H. Derfler, B. Gyorgy, W. Limapichat, S. Walujkar, L. N. Wimalasena, M. Sotomayor, D. P. Corey, J. R. Holt, TMC1 forms the pore of mechanosensory transduction channels in vertebrate inner ear hair cells. *Neuron* **99**, 736–753.e6 (2018).
5. B. Pan, G. S. Geleoc, Y. Asai, G. C. Horwitz, K. Kurima, K. Ishikawa, Y. Kawashima, A. J. Griffith, J. R. Holt, TMC1 and TMC2 are components of the mechanotransduction channel in hair cells of the mammalian inner ear. *Neuron* **79**, 504–515 (2013).
6. C. L. Cunningham, X. Qiu, Z. Wu, B. Zhao, G. Peng, Y. H. Kim, A. Lauer, U. Muller, TMIE defines pore and gating properties of the mechanotransduction channel of mammalian cochlear hair cells. *Neuron* **107**, 126–143.e128 (2020).
7. W. Xiong, N. Grillet, H. M. Elledge, T. F. Wagner, B. Zhao, K. R. Johnson, P. Kazmierczak, U. Muller, TMHS is an integral component of the mechanotransduction machinery of cochlear hair cells. *Cell* **151**, 1283–1295 (2012).
8. R. Maeda, K. S. Kindt, W. Mo, C. P. Morgan, T. Erickson, H. Zhao, R. Clemens-Grisham, P. G. Barr-Gillespie, T. Nicolson, Tip-link protein protocadherin 15 interacts with transmembrane channel-like proteins TMC1 and TMC2. *Proc. Natl. Acad. Sci. U.S.A.* **111**, 12907–12912 (2014).
9. W. Zheng, J. R. Holt, The mechanosensory transduction machinery in inner ear hair cells. *Annu. Rev. Biophys.* **50**, 31–51 (2021).
10. Y. Jia, Y. Zhao, T. Kusakizako, Y. Wang, C. Pan, Y. Zhang, O. Nureki, M. Hattori, Z. Yan, TMC1 and TMC2 proteins are pore-forming subunits of mechanosensitive ion channels. *Neuron* **105**, 310–321.e3 (2019).
11. L. F. Corns, J. Y. Jeng, G. P. Richardson, C. J. Kros, W. Marcotti, TMC2 modifies permeation properties of the mechanoelectrical transducer channel in early postnatal mouse cochlear outer hair cells. *Front. Mol. Neurosci.* **10**, 326 (2017).
12. Y. Kawashima, G. S. Geleoc, K. Kurima, V. Labay, A. Lelli, Y. Asai, T. Makishima, D. K. Wu, C. C. Della Santina, J. R. Holt, A. J. Griffith, Mechanotransduction in mouse inner ear hair cells requires transmembrane channel-like genes. *J. Clin. Invest.* **121**, 4796–4809 (2011).
13. H. Nakanishi, K. Kurima, B. Pan, P. Wangemann, T. S. Fitzgerald, G. S. Geleoc, J. R. Holt, A. J. Griffith, Tmc2 expression partially restores auditory function in a mouse model of DFNB7/B11 deafness caused by loss of Tmc1 function. *Sci. Rep.* **8**, 12125 (2018).
14. Y. Asai, B. Pan, C. Nist-Lund, A. Galvin, A. N. Lukashkin, V. A. Lukashkina, T. Chen, W. Zhou, H. Zhu, I. J. Russell, J. R. Holt, G. S. G. Geleoc, Transgenic Tmc2 expression preserves inner ear hair cells and vestibular function in mice lacking Tmc1. *Sci. Rep.* **8**, 12124 (2018).
15. Y. Kawashima, K. Kurima, B. Pan, A. J. Griffith, J. R. Holt, Transmembrane channel-like (TMC) genes are required for auditory and vestibular mechanosensation. *Pflugers Arch.* **467**, 85–94 (2015).
16. K. Kurima, L. M. Peters, Y. Yang, S. Riazuddin, Z. M. Ahmed, S. Naz, D. Arnaud, S. Drury, J. Mo, T. Makishima, M. Ghosh, P. S. Menon, D. Deshmukh, C. Oddoux, H. Ostrer, S. Khan, S. Riazuddin, P. L. Deininger, L. L. Hampton, S. L. Sullivan, J. F. Battey Jr., B. J. Keats, E. R. Wilcox, T. B. Friedman, A. J. Griffith, Dominant and recessive deafness caused by mutations of a novel gene, TMC1, required for cochlear hair-cell function. *Nat. Genet.* **30**, 277–284 (2002).
17. M. Beurg, A. C. Goldring, R. Fettiplace, The effects of Tmc1 Beethoven mutation on mechanotransducer channel function in cochlear hair cells. *J. Gen. Physiol.* **146**, 233–243 (2015).
18. S. Vreugde, A. Erven, C. J. Kros, W. Marcotti, H. Fuchs, K. Kurima, E. R. Wilcox, T. B. Friedman, A. J. Griffith, R. Balling, M. Hrabe De Angelis, K. B. Avraham, K. P. Steel, Beethoven, a mouse model for dominant, progressive hearing loss DFNA36. *Nat. Genet.* **30**, 257–258 (2002).
19. M. Beurg, A. Barlow, D. N. Furness, R. Fettiplace, A Tmc1 mutation reduces calcium permeability and expression of mechanoelectrical transduction channels in cochlear hair cells. *Proc. Natl. Acad. Sci. U.S.A.* **116**, 20743–20749 (2019).
20. M. Beurg, L. A. Schimmenti, A. Koleilat, S. S. Amr, A. Oza, A. J. Barlow, A. Ballesteros, R. Fettiplace, New Tmc1 deafness mutations impact mechanotransduction in auditory hair cells. *J. Neurosci.* **41**, 4378–4391 (2021).
21. W. Marcotti, A. Erven, S. L. Johnson, K. P. Steel, C. J. Kros, Tmc1 is necessary for normal functional maturation and survival of inner and outer hair cells in the mouse cochlea. *J. Physiol.* **574**, 677–698 (2006).
22. L. F. Corns, S. L. Johnson, C. J. Kros, W. Marcotti, Tmc1 point mutation affects $Ca2^+$ sensitivity and block by dihydrostreptomycin of the mechanoelectrical transducer current of mouse outer hair cells. *J. Neurosci.* **36**, 336–349 (2016).
23. A. Ballesteros, C. Fenollar-Ferrer, K. J. Swartz, Structural relationship between the putative hair cell mechanotransduction channel TMC1 and TMEM16 proteins. *eLife* **7**, e38433 (2018).

24. A. Medrano-Soto, G. Moreno-Hagelsieb, D. McLaughlin, Z. S. Ye, K. J. Hendargo, M. H. Saier Jr., Bioinformatic characterization of the anoctamin superfamily of $Ca2^{+}$-activated ion channels and lipid scramblases. *PLOS ONE* **13**, e0192851 (2018).
25. K. Kunzelmann, I. Cabrita, P. Wanitchakool, J. Ousingsawat, L. Sirianant, R. Benedetto, R. Schreiber, Modulating Ca^{2+} signals: A common theme for TMEM16, Ist2, and TMC. *Pflugers Arch.* **468**, 475–490 (2016).
26. Y. Hahn, D. S. Kim, I. H. Pastan, B. Lee, Anoctamin and transmembrane channel-like proteins are evolutionarily related. *Int. J. Mol. Med.* **24**, 51–55 (2009).
27. V. Kalienkova, V. Clerico Mosina, C. Paulino, The groovy TMEM16 family: Molecular mechanisms of lipid scrambling and ion conduction. *J. Mol. Biol.* **433**, 166941 (2021).
28. E. M. Bevers, P. L. Williamson, Getting to the outer leaflet: Physiology of phosphatidylserine exposure at the plasma membrane. *Physiol. Rev.* **96**, 605–645 (2016).
29. B. C. Lee, A. K. Menon, A. Accardi, The nhTMEM16 scramblase is also a nonselective ion channel. *Biophys. J.* **111**, 1919–1924 (2016).
30. T. Jiang, K. Yu, H. C. Hartzell, E. Tajkhorshid, Lipids and ions traverse the membrane by the same physical pathway in the nhTMEM16 scramblase. *eLife* **6**, e28671 (2017).
31. M. Malvezzi, K. K. Andra, K. Pandey, B. C. Lee, M. E. Falzone, A. Brown, R. Iqbal, A. K. Menon, A. Accardi, Out-of-the-groove transport of lipids by TMEM16 and GPCR scramblases. *Proc. Natl. Acad. Sci. U.S.A.* **115**, E7033–E7042 (2018).
32. R. J. Goodyear, J. E. Gale, K. M. Ranatunga, C. J. Kros, G. P. Richardson, Aminoglycoside-induced phosphatidylserine externalization in sensory hair cells is regionally restricted, rapid, and reversible. *J. Neurosci.* **28**, 9939–9952 (2008).
33. G. P. Richardson, I. J. Russell, Cochlear cultures as a model system for studying aminoglycoside induced ototoxicity. *Hear. Res.* **53**, 293–311 (1991).
34. B. Kotecha, G. P. Richardson, Ototoxicity in vitro: Effects of neomycin, gentamicin, dihydrostreptomycin, amikacin, spectinomycin, neamine, spermine and poly-L-lysine. *Hear. Res.* **73**, 173–184 (1994).
35. M. E. Warchol, A. Schrader, L. Sheets, Macrophages respond rapidly to ototoxic injury of lateral line hair cells but are not required for hair cell regeneration. *Front. Cell. Neurosci.* **14**, 613246 (2020).
36. D. P. Corey, A. J. Hudspeth, Kinetics of the receptor current in bullfrog saccular hair cells. *J. Neurosci.* **3**, 962–976 (1983).
37. E. Glowatzki, J. P. Ruppersberg, H. P. Zenner, A. Rusch, Mechanically and ATP-induced currents of mouse outer hair cells are independent and differentially blocked by d-tubocurarine. *Neuropharmacology* **36**, 1269–1275 (1997).
38. A. Rusch, C. J. Kros, G. P. Richardson, Block by amiloride and its derivatives of mechano-electrical transduction in outer hair cells of mouse cochlear cultures. *J. Physiol.* **474**, 75–86 (1994).
39. A. B. Kroese, A. Das, A. J. Hudspeth, Blockage of the transduction channels of hair cells in the bullfrog's sacculus by aminoglycoside antibiotics. *Hear. Res.* **37**, 203–217 (1989).
40. P. Meers, T. Mealy, Calcium-dependent annexin V binding to phospholipids: Stoichiometry, specificity, and the role of negative charge. *Biochemistry* **32**, 11711–11721 (1993).
41. G. P. Richardson, I. J. Russell, R. Wasserkort, M. Hans, Aminoglycoside antibiotics and lectins cause irreversible increases in the stiffness of cochlear hair-cell stereocilia, in *Cochlear Mechanisms: Structure, Function, and Models,* J. P. Wilson, D. T. Kemp, Eds. (Springer US, 1989), pp. 57–65.
42. A. Ballesteros, T. S. Fitzgerald, K. J. Swartz, Expression of a membrane-targeted fluorescent reporter disrupts auditory hair cell mechanoelectrical transduction and causes profound deafness. *Hear. Res.* **404**, 108212 (2021).
43. H. E. Farris, C. L. LeBlanc, J. Goswami, A. J. Ricci, Probing the pore of the auditory hair cell mechanotransducer channel in turtle. *J. Physiol.* **558**, 769–792 (2004).
44. A. Forge, G. Richardson, Freeze fracture analysis of apical membranes in cochlear cultures: Differences between basal and apical-coil outer hair cells and effects of neomycin. *J. Neurocytol.* **22**, 854–867 (1993).
45. N. Wu, V. Cernysiov, D. Davidson, H. Song, J. Tang, S. Luo, Y. Lu, J. Qian, I. E. Gyurova, S. N. Waggoner, V. Q. Trinh, R. Cayrol, A. Sugiura, H. M. McBride, J. F. Daudelin, N. Labrecque, A. Veillette, Critical role of lipid scramblase TMEM16F in phosphatidylserine exposure and repair of plasma membrane after pore formation. *Cell Rep.* **30**, 1129–1140.e5 (2020).
46. T. W. Han, W. Ye, N. P. Bethel, M. Zubia, A. Kim, K. H. Li, A. L. Burlingame, M. Grabe, Y. N. Jan, L. Y. Jan, Chemically induced vesiculation as a platform for studying TMEM16F activity. *Proc. Natl. Acad. Sci. U.S.A.* **116**, 1309–1318 (2019).
47. S. J. Foltz, Y. Y. Cui, H. J. Choo, H. C. Hartzell, ANO5 ensures trafficking of annexins in wounded myofibers. *J. Cell Biol.* **220**, e202007059 (2021).
48. M. Beurg, R. Fettiplace, J. H. Nam, A. J. Ricci, Localization of inner hair cell mechanotransducer channels using high-speed calcium imaging. *Nat. Neurosci.* **12**, 553–558 (2009).
49. K. Kurima, S. Ebrahim, B. Pan, M. Sedlacek, P. Sengupta, B. A. Millis, R. Cui, H. Nakanishi, T. Fujikawa, Y. Kawashima, B. Y. Choi, K. Monahan, J. R. Holt, A. J. Griffith, B. Kachar, TMC1 and TMC2 localize at the site of mechanotransduction in mammalian inner ear hair cell stereocilia. *Cell Rep.* **12**, 1606–1617 (2015).
50. E. Cocucci, J. Meldolesi, Ectosomes and exosomes: Shedding the confusion between extracellular vesicles. *Trends Cell Biol.* **25**, 364–372 (2015).
51. A. A. Indzhykulian, R. Stepanyan, A. Nelina, K. J. Spinelli, Z. M. Ahmed, I. A. Belyantseva, T. B. Friedman, P. G. Barr-Gillespie, G. I. Frolenkov, Molecular remodeling of tip links underlies mechanosensory regeneration in auditory hair cells. *PLOS Biol.* **11**, e1001583 (2013).
52. Y. Zhao, E. N. Yamoah, P. G. Gillespie, Regeneration of broken tip links and restoration of mechanical transduction in hair cells. *Proc. Natl. Acad. Sci. U.S.A.* **93**, 15469–15474 (1996).
53. A. Lelli, P. Kazmierczak, Y. Kawashima, U. Muller, J. R. Holt, Development and regeneration of sensory transduction in auditory hair cells requires functional interaction between cadherin-23 and protocadherin-15. *J. Neurosci.* **30**, 11259–11269 (2010).
54. K. Del Vecchio, R. V. Stahelin, Investigation of the phosphatidylserine binding properties of the lipid biosensor, Lactadherin C2 (LactC2), in different membrane environments. *J. Bioenerg. Biomembr.* **50**, 1–10 (2018).
55. S. K. Bosher, R. L. Warren, Very low calcium content of cochlear endolymph, an extracellular fluid. *Nature* **273**, 377–378 (1978).
56. E. Gabev, J. Kasianowicz, T. Abbott, S. McLaughlin, Binding of neomycin to phosphatidylinositol 4,5-biphosphate (PIP2). *Biochim. Biophys. Acta* **979**, 105–112 (1989).
57. A. Alharazneh, L. Luk, M. Huth, A. Monfared, P. S. Steyger, A. G. Cheng, A. J. Ricci, Functional hair cell mechanotransducer channels are required for aminoglycoside ototoxicity. *PLOS ONE* **6**, e22347 (2011).
58. D. Raucher, T. Stauffer, W. Chen, K. Shen, S. Guo, J. D. York, M. P. Sheetz, T. Meyer, Phosphatidylinositol 4,5-bisphosphate functions as a second messenger that regulates cytoskeleton–plasma membrane adhesion. *Cell* **100**, 221–228 (2000).
59. A. Lelli, Y. Asai, A. Forge, J. R. Holt, G. S. Geleoc, Tonotopic gradient in the developmental acquisition of sensory transduction in outer hair cells of the mouse cochlea. *J. Neurophysiol.* **101**, 2961–2973 (2009).
60. A. Makabe, Y. Kawashima, Y. Sakamaki, A. Maruyama, T. Fujikawa, T. Ito, K. Kurima, A. J. Griffith, T. Tsutsumi, Systemic fluorescent gentamicin enters neonatal mouse hair cells predominantly through sensory mechanoelectrical transduction channels. *J. Assoc. Res. Otolaryngol.* **21**, 137–149 (2020).
61. H. Yang, A. Kim, T. David, D. Palmer, T. Jin, J. Tien, F. Huang, T. Cheng, S. R. Coughlin, Y. N. Jan, L. Y. Jan, TMEM16F forms a Ca^{2+}-activated cation channel required for lipid scrambling in platelets during blood coagulation. *Cell* **151**, 111–122 (2012).
62. M. Beurg, J. H. Nam, Q. Chen, R. Fettiplace, Calcium balance and mechanotransduction in rat cochlear hair cells. *J. Neurophysiol.* **104**, 18–34 (2010).
63. K. J. Spinelli, P. G. Gillespie, Monitoring intracellular calcium ion dynamics in hair cell populations with fluo-4 AM. *PLOS ONE* **7**, e51874 (2012).
64. A. C. Velez-Ortega, M. J. Freeman, A. A. Indzhykulian, J. M. Grossheim, G. I. Frolenkov, Mechanotransduction current is essential for stability of the transducing stereocilia in mammalian auditory hair cells. *eLife* **6**, e24661 (2017).
65. A. W. Peng, T. Effertz, A. J. Ricci, Adaptation of mammalian auditory hair cell mechanotransduction is independent of calcium entry. *Neuron* **80**, 960–972 (2013).
66. M. Beurg, R. Cui, A. C. Goldring, S. Ebrahim, R. Fettiplace, B. Kachar, Variable number of TMC1-dependent mechanotransducer channels underlie tonotopic conductance gradients in the cochlea. *Nat. Commun.* **9**, 2185 (2018).
67. D. N. Furness, S. L. Johnson, U. Manor, L. Ruttiger, A. Tocchetti, N. Offenhauser, J. Olt, R. J. Goodyear, S. Vijayakumar, Y. Dai, C. M. Hackney, C. Franz, P. P. Di Fiore, S. Masetto, S. M. Jones, M. Knipper, M. C. Holley, G. P. Richardson, B. Kachar, W. Marcotti, Progressive hearing loss and gradual deterioration of sensory hair bundles in the ears of mice lacking the actin-binding protein Eps8L2. *Proc. Natl. Acad. Sci. U.S.A.* **110**, 13898–13903 (2013).
68. L. L. Cunningham, A. G. Cheng, E. W. Rubel, Caspase activation in hair cells of the mouse utricle exposed to neomycin. *J. Neurosci.* **22**, 8532–8540 (2002).
69. P. Majumder, P. A. Moore, G. P. Richardson, J. E. Gale, Protecting mammalian hair cells from aminoglycoside-toxicity: Assessing phenoxybenzamine's potential. *Front. Cell. Neurosci.* **11**, 94 (2017).
70. N. K. Kirkwood, M. O'Reilly, M. Derudas, E. J. Kenyon, R. Huckvale, S. M. van Netten, S. E. Ward, G. P. Richardson, C. J. Kros, d-Tubocurarine and berbamine: Alkaloids that are permeant blockers of the hair cell's mechano-electrical transducer channel and protect from aminoglycoside toxicity. *Front. Cell. Neurosci.* **11**, 262 (2017).
71. A. J. Ricci, R. Fettiplace, Calcium permeation of the turtle hair cell mechanotransducer channel and its relation to the composition of endolymph. *J. Physiol.* **506**, 159–173 (1998).
72. A. Forge, S. Davies, G. Zajic, Characteristics of the membrane of the stereocilia and cell apex in cochlear hair cells. *J. Neurocytol.* **17**, 325–334 (1988).
73. R. Fettiplace, J. H. Nam, Tonotopy in calcium homeostasis and vulnerability of cochlear hair cells. *Hear. Res.* **376**, 11–21 (2019).
74. L. F. Corns, S. L. Johnson, C. J. Kros, W. Marcotti, Calcium entry into stereocilia drives adaptation of the mechanoelectrical transducer current of mammalian cochlear hair cells. *Proc. Natl. Acad. Sci. U.S.A.* **111**, 14918–14923 (2014).

75. M. Hirono, C. S. Denis, G. P. Richardson, P. G. Gillespie, Hair cells require phosphatidylinositol 4,5-bisphosphate for mechanical transduction and adaptation. *Neuron* **44**, 309–320 (2004).
76. T. Effertz, L. Becker, A. W. Peng, A. J. Ricci, Phosphoinositol-4,5-bisphosphate regulates auditory hair-cell mechanotransduction-channel pore properties and fast adaptation. *J. Neurosci.* **37**, 11632–11646 (2017).
77. A. C. Goldring, M. Beurg, R. Fettiplace, The contribution of TMC1 to adaptation of mechanoelectrical transduction channels in cochlear outer hair cells. *J. Physiol.* **597**, 5949–5961 (2019).
78. J. Suzuki, E. Imanishi, S. Nagata, Xkr8 phospholipid scrambling complex in apoptotic phosphatidylserine exposure. *Proc. Natl. Acad. Sci. U.S.A.* **113**, 9509–9514 (2016).
79. M. E. Falzone, J. Rheinberger, B. C. Lee, T. Peyear, L. Sasset, A. M. Raczkowski, E. T. Eng, A. Di Lorenzo, O. S. Andersen, C. M. Nimigean, A. Accardi, Structural basis of Ca^{2+}-dependent activation and lipid transport by a TMEM16 scramblase. *eLife* **8**, e43229 (2019).
80. Y. E. Li, Y. Wang, X. Du, T. Zhang, H. Y. Mak, S. E. Hancock, H. McEwen, E. Pandzic, R. M. Whan, Y. C. Aw, I. E. Lukmantara, Y. Yuan, X. Dong, A. Don, N. Turner, S. Qi, H. Yang, TMEM41B and VMP1 are scramblases and regulate the distribution of cholesterol and phosphatidylserine. *J. Cell Biol.* **220**, e202103105 (2021).
81. K. Matoba, T. Kotani, A. Tsutsumi, T. Tsuji, T. Mori, D. Noshiro, Y. Sugita, N. Nomura, S. Iwata, Y. Ohsumi, T. Fujimoto, H. Nakatogawa, M. Kikkawa, N. N. Noda, Atg9 is a lipid scramblase that mediates autophagosomal membrane expansion. *Nat. Struct. Mol. Biol.* **27**, 1185–1193 (2020).
82. M. A. Goren, T. Morizumi, I. Menon, J. S. Joseph, J. S. Dittman, V. Cherezov, R. C. Stevens, O. P. Ernst, A. K. Menon, Constitutive phospholipid scramblase activity of a G protein-coupled receptor. *Nat. Commun.* **5**, 5115 (2014).
83. M. Magarinos, S. Pulido, M. R. Aburto, R. de I. Rodriguez, I. Varela-Nieto, Autophagy in the vertebrate inner ear. *Front. Cell Dev. Biol.* **5**, 56 (2017).
84. H. Liu, J. L. Pecka, Q. Zhang, G. A. Soukup, K. W. Beisel, D. Z. He, Characterization of transcriptomes of cochlear inner and outer hair cells. *J. Neurosci.* **34**, 11085–11095 (2014).
85. E. Mailler, C. M. Guardia, X. Bai, M. Jarnik, C. D. Williamson, Y. Li, N. Maio, A. Golden, J. S. Bonifacino, The autophagy protein ATG9A enables lipid mobilization from lipid droplets. *Nat. Commun.* **12**, 6750 (2021).
86. H. Nakanishi, K. Kurima, Y. Kawashima, A. J. Griffith, Mutations of TMC1 cause deafness by disrupting mechanoelectrical transduction. *Auris Nasus Larynx* **41**, 399–408 (2014).
87. J. M. Stapelbroek, T. A. Peters, D. H. van Beurden, J. H. Curfs, A. Joosten, A. J. Beynon, B. M. van Leeuwen, L. M. van der Velden, L. Bull, R. P. Oude Elferink, B. A. van Zanten, L. W. Klomp, R. H. Houwen, ATP8B1 is essential for maintaining normal hearing. *Proc. Natl. Acad. Sci. U.S.A.* **106**, 9709–9714 (2009).
88. J. F. Krey, P. Chatterjee, R. A. Dumont, M. O'Sullivan, D. Choi, J. E. Bird, P. G. Barr-Gillespie, Mechanotransduction-dependent control of stereocilia dimensions and row identity in inner hair cells. *Curr. Biol.* **30**, 442–454.e7 (2020).
89. E. J. Kenyon, N. K. Kirkwood, S. R. Kitcher, R. J. Goodyear, M. Derudas, D. M. Cantillon, S. Baxendale, A. de la Vega de Leon, V. N. Mahieu, R. T. Osgood, C. D. Wilson, J. C. Bull, S. J. Waddell, T. T. Whitfield, S. E. Ward, C. J. Kros, G. P. Richardson, Identification of a series of hair-cell MET channel blockers that protect against aminoglycoside-induced ototoxicity. *JCI Insight* **6**, e145704 (2021).
90. C. R. Wood, J. L. Rosenbaum, Ciliary ectosomes: Transmissions from the cell's antenna. *Trends Cell Biol.* **25**, 276–285 (2015).
91. V. P. Bhavanandan, A. W. Katlic, The interaction of wheat germ agglutinin with sialoglycoproteins. The role of sialic acid. *J. Biol. Chem.* **254**, 4000–4008 (1979).

Acknowledgments: We thank J. Diamond, C. Weisz, R. Fettiplace, and members of the Swartz laboratory and colleagues for helpful discussions and feedback and H. Chang for support with the mouse colony. We also thank A. Griffith, W. Chien, and R. Fettiplace for sharing the *Tmc* transgenic mice with us, and L. Chernomordik for providing the Lact-C2 plasmid and purification protocol. We thank V. Schram in the NICHD Microscopy and Imaging Core for assistance and feedback with imaging. **Funding:** This research was supported by the Intramural Research Programs of the National Institute of Neurological Disorders and Stroke, NIH, Bethesda, MD to K.J.S. (NS002945). **Author contributions:** Conceptualization: A.B. and K.J.S. Methodology: A.B. Investigation: A.B. Funding acquisition: K.J.S. Supervision: A.B. and K.J.S. Writing—original draft: A.B. Writing—review and editing: A.B. and K.J.S. **Competing interests:** The authors declare that they have no competing interests. **Data and materials availability:** All data needed to evaluate the conclusions in the paper are present in the paper and/or the Supplementary Materials. The *Tmc1*$^{D569N/D569N}$ and *Tmc1*$^{D528N/D528N}$ mutant mice can be provided by R. Fettiplace pending scientific review and a completed material transfer agreement. Requests for *Tmc1*$^{D569N/D569N}$ and *Tmc1*$^{D528N/D528N}$ should be submitted to R. Fettiplace.

Submitted 4 October 2021
Accepted 21 June 2022
Published 3 August 2022
10.1126/sciadv.abm5550